

## **Vestiges of older greenstone in Mesoarchean Chakradharpur granite gneiss, Singhbhum Craton, India: implications for plume-lithosphere interaction at rifted cratonic margin**

**Naresh C. Ghose<sup>1,2</sup>, Abhishek Saha<sup>3\*</sup>**

<sup>1</sup>G/608, Raheja Residency, Koramangala, Bangalore 560 034, India

<sup>2</sup>Department of Geology, Patna University, Patna 800 005, India

<sup>3</sup>CSIR-National Institute of Oceanography, Dona Paula, Goa 403 004, India

\*Corresponding author: Email: asaha.nio2015@gmail.com

### **Abstract**

The Chakradharpur Granite Gneiss (CGG) represents an uplifted Archean basement within the North Singhbhum Orogen (NSO) of Singhbhum-Orissa Craton in the eastern Indian shield and shares a Mesoarchean 3.12 Ga age equivalent to the emplacement of Singhbhum Granite (SBG) phase III. The CGG hosts numerous enclaves of tonalitic gneisses, metamorphosed ultramafic and mafic volcanics, metagabbros, metasediments and conglomerates that collectively represent vestiges of an older greenstone belt preserved within it. The mineralogical composition of the ultramafic volcanics enclaves of CGG has been overprinted by greenschist facies metamorphism presenting a talc-tremolite-phlogopite-actinolite assemblage with prominent development of crenulation cleavage, pressure solutions and relict spinifex texture. These are characterized by restricted low SiO<sub>2</sub> (39.7-46.8 wt.%) at consistently high MgO (20.7-28 wt.%) contents, and geochemically classified as: (i) subalkaline (Na<sub>2</sub>O + K<sub>2</sub>O < 2) komatiite and meimechite, and (ii) an alkaline (Na<sub>2</sub>O + K<sub>2</sub>O > 2) type picobasalt-foiidite-basanite assemblage. Depleted LILE and LREE chemistry, Al<sub>2</sub>O<sub>3</sub>/TiO<sub>2</sub> vs. (Gd/Yb)<sub>N</sub> and HFSE abundances suggest that the studied Al-undepleted Munro-type komatiite and meimechite were derived by high degree (30%-50%), shallow level (<90 km) partial melting of a hot, anhydrous mantle plume carrying depleted components. It is suggested that the komatiite-meimechite melts were deflected by an Archean cratonic keel and erupted through thinned continental lithosphere at a rifted cratonic margin. Geochemical evidence of crustal contamination preserved in these komatiites are equated with minor input from reworking of older continental materials and interaction between plume-derived asthenospheric melts and metasomatized sub-continental lithospheric mantle (SCLM). Zr/Hf, Zr/Sm, Nb/Ta, Zr/Nb and Nb/Th ratios for the picobasalt, high-Mg basalt, foidite and basanite rocks, and corroborate their generation through variable degrees of partial melting of a heterogeneous lithospheric mantle source carrying depleted plume-derived melts and enriched components from metasomatized lithosphere. Mantle processes involved assimilation of metasomatic components of SCLM by ascending melts of plume incubating at the base of lithosphere ensued by melt generation at different mantle depths extending from garnet to spinel peridotite domains. Therefore, the geochemical signatures of ultramafic enclaves in CGG invoke distinct magmatic episodes during plume-craton interaction, melt generation at thinned craton margin to rifted continental interior and melting of metasomatized continental lithosphere that collectively contributed to the evolution of Archean mantle-lithosphere system, volcanism with diverse chemical compositions and greenstone generation in the Singhbhum Craton.

**Keywords:** Chakradharpur granites; enclaves; Singhbhum Craton; komatiite; ultramafic-alkaline; plume-craton interaction

## 1. Introduction

Archean Cratons occurring across the globe represent collages of ancient oceanic plateaus, subduction-accretion complexes, arc-continent collisions, ocean basin closures that reflect distinct magmatic and tectonic processes attributing to crustal growth, evolution of lithosphere-asthenosphere system and cyclic episodes of amalgamation and disintegration of microcontinents during the early evolution of the earth (Condie and Kroner, 2013; Dostal and Mueller 2013; Santosh, 2013; Zhai and Santosh, 2013; Ganguly and Yang, 2018). Accretion of island arc and oceanic plateaus have been proposed as viable models for lateral growth of continental crust. However, mantle plume activities in terms of ocean island basalts (OIB), oceanic plateau basalts (OPB), continental flood basalts (CFB) and underplating of plume-derived melts beneath lower crust account for vertical crustal growth (Condie, 1999; Turkina and Nozkhin, 2003; Bedard, 2018; Wyman, 2018). The Archean granite-greenstone belts nested in ancient cratonic nuclei of continents all over the world such as the Superior Province, Canada; Kaapval Craton, South Africa; Pilbara Craton, Australia; North China Craton; Baltic Shield, Russia; Dharwar, Bastar, Bundelkhand, Aravalli and Singhbhum Cratons in Peninsular India are composed of various lithological assemblages which preserve distinct geological and geochemical signatures of episodic continental growth during Precambrian times through varying conditions of magma generation with vertical and lateral accretion of juvenile crustal materials under different geodynamic processes in oceanic or continental settings (Kerrick et al., 1999; Smithies et al., 2003, 2009; Polat, 2012; Manikyamba et al., 2017).

Two major types of volcanic rock associations have been documented from Archean greenstone belts: (i) an oceanic plateau association composed of compositionally uniform komatiites and Mg- to Fe-rich tholeiitic basalts erupted from mantle plumes, and (ii) a compositionally diverse intra-oceanic island arc association, dominated by 'normal' tholeiitic to calc-alkaline basalts, andesites, dacites, and rhyolites with boninites, picrites, low-Ti tholeiites, adakites, high magnesian andesites, and Nb-enriched basalts (Polat and Kerrich, 2006). These diverse magmatic suites are juxtaposed in most of the greenstone terranes through subduction-accretion processes (Polat et al., 1999; Kusky and Polat, 1999; Polat et al., 2002; Dostal and Mueller, 2013; Manikyamba et al., 2005; Smithies et al., 2005; Saha et al., 2015). The association of plume magmatism with calc-alkaline intermediate to felsic volcanic rocks has been ascribed to plume-arc interaction in convergent margin settings (Barnes and Van Kranendonk, 2014, Manikyamba and Kerrich, 2012). A third type of volcanic assemblage, although sparse in occurrence compared to the other two types, marked by ultramafic-alkaline lithologies has been studied from Archean greenstone belts indicating plume magmatism at rifted cratonic margins (Manikyamba and Kerrich, 2012).

The elevated geothermal gradients, higher heat production and extensive melting of primitive mantle played pivotal roles in Precambrian ultramafic-mafic magmatism and its contribution towards juvenile crustal growth in diverse tectonic regimes (Rollinson, 2007; Kamber, 2015; Condie and Kroner, 2013; Dostal and Mueller 2013; Santosh, 2013; Zhai and Santosh, 2011, 2013; Ahmad et al., 2008; Reagan et al., 2008). Geochemical compositions of mantle-derived ultramafic-mafic magmas are controlled by (i) the nature of the mantle source (ii) melt extraction process and extent of metasomatism (iii) the conditions of mantle melting including the degree and depth of partial melting (iv) crustal assimilation and fractional crystallization processes during the ascent and emplacement of magma (Arndt et al., 2005; Ray et al., 2013; Saha et al., 2017, 2018). The emplacement mechanisms for ultramafic-mafic magmas form major pathways for the transfer of magma in the upper crust and provide vital evidence for distinct episodes of continent generation and crustal evolution. The origin of high-MgO magmas, viz., komatiites, komatiitic basalts, picrites, picrobasalts, boninites, kimberlites, meimechites, foidites, basanites is attributed to mantle sources that have been depleted, refractory or enriched, unusually hot, anhydrous or rich in volatiles with variations in degrees and depths of melting (Arndt and Nisbet, 1982; Arndt, 2003). The contrasting mechanisms for generation of high-MgO magmas in different tectonic settings provide valuable constraints on the dynamic mantle processes. Komatiites are ultramafic (MgO > 18 wt.%) volcanic rocks that predominantly occur in Archean greenstone belts (Arndt and Nisbet, 1982; Arndt, 2003; Furnes et al., 2013) with much lesser Phanerozoic occurrences. Archean komatiites are considered to have been derived by high degrees (<30-50%) of partial melting at great depths under 3-10 GPa melting pressures within hot and dry mantle plumes (Herzberg, 1992; Ohtani et al., 1989; Campbell and Griffiths, 1990; Sproule et al., 2002). Meimechites are ultramafic magmas with higher TiO<sub>2</sub> than komatiites and commonly originate from plume melts or deep source asthenospheric melts in an intraplate setting (Arndt, 2003). The mineralogical and geochemical diversity recorded in alkaline ultramafic-mafic magmas has been attributed to variable interactions of plume-derived asthenospheric melts, depleted mantle components, melts from metasomatised sub-continental lithospheric mantle and veined lithospheric mantle pooled in crustal magma chambers which corroborate episodic temporal evolution of differentiated alkaline magmas erupted in rift-controlled intraplate settings in oceanic and continental realms. The ultramafic-mafic lithological assemblages of CGG from the Singhbhum craton in the eastern Indian shield preserves signatures of magmatic and tectonic activities associated with Archean crustal growth and rapid evolution of continental lithosphere during Proterozoic.

This paper involves petrological and geochemical studies of the ultramafic magmatic enclaves of diverse compositions in the Chakradharpur granite gneiss (CGG) at the northwestern periphery of

the Singhbhum Craton with an aim to address (i) petrogenetic aspects (ii) mantle processes and geodynamic conditions operative during their origin (iii) their analogy with Archean greenstones and (iv) their role in crustal growth and continental lithosphere evolution.

## **2. Regional Geology**

The Singhbhum Craton (Figure 1) is one of the oldest Paleo-Mesoarchean Cratons in the eastern India Shield where the granitoids and their enclaves comprise the oldest component of “Singhbhum nucleus” which is surrounded by volcano-sedimentary associations of supracrustal sequences (Table 1; Naqvi and Rogers, 1987; Saha, 1994; Weaver, 1990; Bose, 2009; Manikyamba et al., 2015; Singh et al., 2015, 2016). The Singhbhum Craton is separated by the E-W trending North Singhbhum Mobile Belt (NSMB) from the Chotanagpur Gneissic Complex (CGC) in the north. The Sukinda thrust and the Gondwana boundary fault of the Talchir coalfield mark the southern boundary of this Craton separating it from the Proterozoic Eastern Ghat Mobile Belt (EGMB). The Bastar Craton lies to the west and is separated from Singhbhum Craton by the Mahanadi Rift. The eastern part of the Singhbhum Craton is covered with the alluvium of the Bengal basin (Dunn and Dey, 1942; Saha, 1994; Mukhopadhyay, 2001; Misra, 2006; Misra and Johnson 2005; Sharma, 2009; Mohanty, 2012). Based on geochronological data, Mohanty (2012) classified the Archean granite greenstone terranes and Proterozoic supracrustals of the Singhbhum Craton (Figure 1) into seven principal units such as 1) the Older Metamorphic Group (OMG), 2) Older Metamorphic Tonalite Gneiss (OMTG), 3) older granite-greenstone belts containing banded iron formation (BIF) of the Gorumahisani-Badampahar-Daitari Iron Ore Group, 4) three phases of plutonic intrusions of Singhbhum granites (SBG I, II and III) 5) two units of younger greenstone belts of Dalma-Dhanjori-Simplipal Group, 6) younger granites and 7) mafic dyke swarms (Newer Dolerite dyke). The OMG constitutes the oldest supracrustal assemblage in the Singhbhum Craton with zircon U-Pb ages clustering at ~3.55 - 3.44 Ga (Basu et al., 1981; Moorbath et al., 1986; Sengupta et al., 1991). The OMG rocks are exposed in and around Champua and Noamundi areas of the Singhbhum Craton (Figure 1) and consists of amphibolite facies pelitic schists, quartz-magnetite-cummingtonite schists, quartzites, banded calc-gneiss, and ortho- and para amphibolites. The OMG amphibolites yielded Sm-Nd whole rock isochron age of  $3305 \pm 60$  Ma (Sharma et al., 1994). The OMG rocks occur as enclaves within the OMTG that is composed of tonalite-trondhjemite-granodiorite (TTG) rocks with zircon U-Pb age of ~3.44-3.42 Ga. However, a Sm-Nd age of ~3.8 Ga has also been proposed for the OMTG indicating the time of generation of parent melt and its subsequent crystallization at the base of the crust (Basu et al., 1981; Moorbath et al., 1986). Previous geochronological studies have suggested 3.52-3.44 Ga igneous crystallization age for the tonalities of OMTG (Roy and Bhattacharya, 2012; Acharyya et al., 2010a,b). Recent ion microprobe U-Pb zircon

dating of tonalite and trondhjemite samples of OMTG has extended the igneous crystallization age up to 3.3 Ga (Nelson et al., 2014). The structural unity between the OMG and OMTG, the migmatitic nature of the OMG enclaves concordant thin injections of tonalite within OMG, parallelism of foliation in OMG and OMTG have led to the conclusion that the OMTG was emplaced synkinematically with the deformation and metamorphism of the OMG (Misra, 2006; Mukhopadhyay, 2001; Misra and Johnson, 2005). The formation of OMG and OMTG were succeeded by two phases of intrusions of granitoid plutons (SBG I: ~3.44–~3.38 Ga; SBG II: ~3.33–3.3 Ga; Misra, 2006; Misra et al., 1999), deposition and deformation of IOG supracrustals and emplacement of SBG III. Zircon U-Pb SHRIMP dating of dacite lavas from IOG supracrustal of Daitari yield an age of  $3508 \pm 2$  Ma while 3.4 Ga U-Pb zircon age has been reported for the IOG volcanic rocks of Noamundi-Koira valley (Mukhopadhyay et al., 2008). The deformation, metamorphism and migmatization of the Iron ore orogeny at 3.35–3.3 Ga overprinted the older sequences of the Singhbhum Craton and were followed by rifting and emplacement of mafic dykes (Mohanty, 2012). The SBG II contains enclaves of OMG and OMTG whereas IOG enclaves are only present within SBG III which was emplaced during 3.3–3.1 Ga. SBG III including the Bonai granite, Katipada granite, Chakradharpur granite are the most abundant among the three phases of Singhbhum granite. The emplacement of SBG II and III was punctuated by the formation of IOG basins (Saha, 1994; Mukhopadhyay, 2001).

The Singhbhum-Orissa Craton in the eastern Indian shield attained stability at 3.1 Ga that corresponds to the age of Singhbhum Granite (SBG) phase III (Mukhopadhyay, 2001; Sharma, 2009). The Chakradharpur Granite Gneiss (CGG) occurring near the northern end of the Noamundi synclinorium represents an uplifted Archean basement to the south of the Singhbhum Shear Zone (SSZ). The Mesoarchean Chakradharpur granite gneiss (CGG; Figure 2) is a composite body, representing two phases of granitic activity— the earlier one is tonalitic while the later varies in composition from granodiorite to granite (Bandyopadhyay, 1981; 1983). The rocks have undergone folding, mylonitization and refolding of the mylonitized bands (Sharan, 1983). The Chakradharpur granite (225 km<sup>2</sup>) forms a major phase of Precambrian granitic activity, lying between the southern margin of the Singhbhum Mobile Belt (SMB) and the low-grade metamorphites of the Iron Ore group (IOG) in the northern part of the >3400 Ma Older Metamorphic Group of Singhbhum Craton (Saha 1994; Figure 1). The Chakradharpur granite is separated from the IOG by a thick horizon of polymictic conglomerate with an arkosic matrix. A close scrutiny of arkosic material within conglomerate alongside the granite contact, in an otherwise argillaceous terrain to its south (IOG), raises question about its source, and points to possibility of existence of a granitic ensialic basement.

## **2.1 Enclaves in the Chakradharpur granite gneiss (CGG)**

The CGG (Figure 2) contains numerous enclaves/rafts of varied mineralogical composition, viz., metasediments, gneisses (tonalitic), metabasic and meta ultramaficrocks (e.g., komatiite, Ghose et al., 1984) that provide valuable information on the nature of primordial crust. A detailed study of these enclaves collectively suggests that they belong to 'Archean greenstones' that along with gneisses characterize all cratonic areas of the world. The tonalite gneisses are most abundant among various rock types which occur as enclaves within the CGG ranging in composition from tonalite to granodiorite. These gneisses preserve evidence of their involvement in migmatization prior to exhumation. The gneissic enclaves are comparable with the Older Metamorphic Group (OMG) and OMTG (Older metamorphic tonalitic gneisses) of Singbhum (Saha, 1994) and Barberton of South Africa (Viljoen and Viljoen, 1969). The metasedimentary enclaves largely belong to the IOG and include quartz-sericite schist and a mylonitised quartzo-feldspathic rock (Sharan, 1983). At the central part of Chakradharpur granite an enclave of conglomerate has been encountered which forms a special significance in correlating the nature and composition of the sub-crustal rocks.

## **3. Sampling And Analytical Techniques**

Sample locations for the studied rocks types are given in Figure 2. Selected samples devoid of surface alteration or weathering were powdered using agate mortar. Ultramafic volcanic rocks along with matrix matching geochemical reference materials for quality control were analysed for major, trace and REE compositions at CSIR-National Geophysical Research Institute (NGRI), Hyderabad. Major element concentrations were determined by X-ray fluorescence spectrometry (XRF; Phillips MAGIX PRO Model 2440), on pressed pellets prepared from powdered whole-rock samples following the method of Krishna et al. (2007). Pressed pellets (40 mm diameter) were prepared by using collapsible aluminium cups (10). These cups were filled with boric acid and about 2 g of the finely powdered sample was evenly sprayed and pressed under a hydraulic press at 25-ton pressure to get a pellet (Hydraulic Press, Herzog, Germany). Precision for different elements is referred to the reported values of Manikyamba et al. (2014a). The trace elements including rare earth elements (REE) were analyzed by employing closed digestion method. The powdered samples were digested by adding double distilled acids HF:HNO<sub>3</sub> at a ratio of 7:3 to 0.05 g of rock powder in a Savillex<sup>®</sup> vessel. This mixture was kept on hot plate at 150°C for 48 hours. After 48 hours of sample digestion, the solutions were mixed with 1 ml of HClO<sub>4</sub> and kept for evaporation. When the mixture is completely dried, 20 ml of 1:1 HNO<sub>3</sub> was added and kept on hotplate at 70°C for 10-15 minutes till the clear solution is obtained. Then 5 ml of Rhodium (1ppm concentration) was added as an internal standard and kept for cooling. After cooling the solution was made into 250 ml. 10 ml aliquot of the prepared solution was further

diluted to 100 ml to achieve total dissolved solids < 200 ng/g for analytical requirements. Certified reference materials UB-N and BHVO-1 obtained from Geological Survey of France and United States Geological Survey were also treated in the same way as the samples to minimize errors from reagents. All sample and standard solutions were analyzed at CSIR-NGRI, Hyderabad, using high resolution inductively coupled mass spectrometer (HR-ICP-MS) (Nu Instruments Attom, UK) in jump-wiggle mode which permits the analytes of interest to be measured accurately. Solutions were introduced through standard Meinhard<sup>®</sup> nebulizer with a cyclonic spray chamber housed in Peltier cooling system. All quantitative measurements were performed using the instrument software (Attolab v.1), while the data processing was done using Nu Quant<sup>®</sup>, which uses knowledge-driven routines in combination with numerical calculations (quantitative analysis) to perform an automated/manual interpretation of the spectrum of interest. <sup>103</sup>Rh was used as an internal standard and external drift was corrected. Instrument response was corroborated relative to two independent digestions of UB-N and BHVO-1. Precision and reproducibility obtained for international reference materials UB-N and BHVO-1 are found to be better than 2% RSD for majority of the trace elements. The CGG rock samples analyzed in this study have LOI ranging from 0.99 to 7.69 wt.%.

## **4. Results**

### **4.1 Petrography of ultramafic-mafic enclaves**

#### **4.1.1 Ultramafic enclaves**

The ultramafic enclaves are characterized by prominent schistosity with randomly oriented prismatic crystals and fibers of actinolite cross-cut by a few needles of tremolite (Figure 3A) showing relict igneous texture corresponding to ultramafic rock of komatiitic composition. Tremolite-actinolite schist also shows oval-shaped porphyroblast of phlogopite rimmed with titanite (Figure 3B). Random orientation of tremolite and actinolite in these ultramafic enclaves indicate igneous protolith (Figure 3C). Primary clinopyroxene is altered to amphibole with deformation of cleavages in ultramafic enclaves. Talc is derived from alteration of magnesium-rich parent mineral (Figure 3D).

These rocks show a wide range in granularity with coarse-grained amphibole-rich type possibly derived from monomineralic rocks of pyroxenite precursor. Some of these are associated with talc (on alteration of olivine) with poikilitic texture containing amphiboles within talc and relate these to be wehrlite. The coarser ones commonly contain curved cummingtonite, hornblende, talc, serpentinite with calcite and chlorite representing igneous sole (Figures 3E and 3F). The fine-grained ultramafics show a variety of textures from random-isotropic, mat-type to dendritic-spinifex with crenulation cleavages and pressure solutions (Figures 3G and 3H). Mineralogically, these are composed of low-

grade minerals such as talc, tremolite, phlogopite, actinolite, titanite, chlorite, epidote and serpentine derived from peridotitic parent compositions (Figures 3A, B, C, D). Some samples contains minor amounts of plagioclase (albite, <10%) and biotite as well.

#### **4.1.2 Mafic enclaves**

Megascopically, the mafic enclaves are greenish in colour and the texture varies from fine-grained schistose to, massive, coarse-grained gabbroic types. Presence of low-temperature mineral paragenesis, viz., chlorite, talc, tremolite, actinolite along with albite and epidote indicate that these are crystallised under greenschist facies. The amphiboles form the most dominating constituent as long prisms and coarse plates, altering to secondary minerals.

The mafic rocks are essentially composed of plagioclase and amphibole with subordinate amounts of clinopyroxenes, orthopyroxenes, chlorite, sphene, epidote, sericite, ilmenite and magnetite. They vary in grain size from coarse- to fine- types; the coarser (metagabbros) variety shows intergranular to sub-ophitic (Figure 3I), nematoblastic and intersertal textures, with micro-folding and curved cleavages in amphiboles. Plagioclase occurs as inclusions in amphiboles derived from pyroxenes. The plagioclases of gabbroids are andesine ( $An_{35}-An_{42}$ ), compared those associated with the ultramafic rocks are albite ( $An_{7-5}$ ) (Ghose et al., 1984).

#### **4.2 Geochemical characterization and Nomenclature of ultramafic enclaves**

A comparison of texture and mineralogy of the mafic and ultramafic enclaves indicates that they belong to high-Mg precursor of an Archean greenstone terrane. The high-Mg volcanic rocks of have been classified on the basis of their total alkali ( $Na_2O + K_2O$ ) vs. silica ( $SiO_2$ ) variations (Le Bas, 2000).  $SiO_2$  contents of the studied samples exhibit a narrow compositional range varying between 39.7 and 46.8 wt.% with consistent elevated concentrations of MgO ranging from 20.74 wt.% to 28.14 wt. % (Table 2). However, rocks having  $Na_2O + K_2O < 2$  plot in the field of komatiite and meimechite, while those with  $Na_2O + K_2O > 2$  occupy the fields of microbasalt, basalt, foidite and basanite in total alkali vs. silica (TAS) diagram (Figure 4) thereby reflecting a subalkaline to alkaline compositional spectrum. Therefore, based on their geochemical characteristics, the komatiite and meimechite are designated as sub-alkaline ultramafic rocks while, the microbasalt, high-Mg basalt, foidite and basanite are grouped as alkaline ultramafic rocks. Komatiite and meimechite show > 18 wt.% MgO contents, however the former is characterized by < 1 wt.%  $TiO_2$ , while the latter contains > 1 wt.%  $TiO_2$  (Figure 4; Table 2).



#### 4.2.1 Major element chemistry

##### *Komatiite and Meimechite*

Major element chemistry of the komatiite and meimechite is characterized by low to moderate SiO<sub>2</sub> (41-45.4 wt. %), moderate Al<sub>2</sub>O<sub>3</sub> (10.5-11.62 wt. %), Fe<sub>2</sub>O<sub>3</sub> (8.7-10.21 wt. %), low CaO (2-6 wt.%), MnO (0.1 wt. %), P<sub>2</sub>O<sub>5</sub> (0.03-0.1 wt.%) and total alkali (Na<sub>2</sub>O +K<sub>2</sub>O= 0.1-0.56 wt. %) contents. The komatiite and meimechite characteristically show 0.1 wt. % and 1.15 wt. % TiO<sub>2</sub> at 28.14 wt.% and 24.8 wt.% MgO respectively. The komatiite sample (sample CG 80/44 : Al<sub>2</sub>O<sub>3</sub>/TiO<sub>2</sub>= 116.22 and CaO/Al<sub>2</sub>O<sub>3</sub>=0.6, Table 2) is analogous to Al-undepleted Munro type komatiite.

##### *Picrobasalt and High-Mg basalt*

The picrobasalts are distinguishable by lower SiO<sub>2</sub> (42.7 wt.%), Al<sub>2</sub>O<sub>3</sub>(9.01 wt. %), and higher CaO (8.7 wt. %), MgO (23.84 wt.%) and TiO<sub>2</sub> (1.9 wt.%) contents than the high-Mg basalts (SiO<sub>2</sub> : 46.8 wt.%, Al<sub>2</sub>O<sub>3</sub>: 15.9 wt. %, CaO : 0.14 wt. %, MgO : 20.74 wt.% and TiO<sub>2</sub> : 1.1 wt.%). The high Mg basalt sample is enriched in total alkalis and iron in comparison with the picrobasalt (Table 2).

##### *Foidite*

The foidites show distinct alkaline composition with narrow compositional range of SiO<sub>2</sub> (39.72 to 40.57 wt. %), medium TiO<sub>2</sub> varying between 0.5 and 1.1 wt.%, moderate Al<sub>2</sub>O<sub>3</sub> ranging from 9.3-10.6 wt.%, moderate Fe<sub>2</sub>O<sub>3</sub> in the range of 8.6 and 9.54 wt. %, low MnO (0.11-0.13 wt. %), and P<sub>2</sub>O<sub>5</sub> (0.1wt.%) with characteristically high MgO (24.6-24.9 wt.%) and total alkali contents (2.14-2.25 wt.%).

##### *Basanite*

The basanites are characterized by 41.4-44.8 wt. % SiO<sub>2</sub>, 0.34 -1.3 wt.% TiO<sub>2</sub>, 8.53-13.43 wt.% Al<sub>2</sub>O<sub>3</sub>, 7.4-9.51 wt. % Fe<sub>2</sub>O<sub>3</sub>, 23-24.68 wt. % MgO, 4.84-9.82 wt.% CaO, 0.1-0.14 wt. % MnO and 0.1-0.28 wt.% P<sub>2</sub>O<sub>5</sub>. The higher total alkali contents (3.05-3.87 wt.%) than the picrobasalts. An ultramafic rock with alkaline affinity is confirmed by low SiO<sub>2</sub> and high MgO contents.

#### 4.2.2 Trace and rare earth element chemistry

##### *Komatiite and Meimechite*

Compatible trace element compositions for the komatiite and meimechite are characterized by 258 and 143 ppm Ni, 50 and 51 ppm Co and 1122 and 171 ppm Cr respectively. Incompatible large ion lithophile elements (LILE), and high-field strength elements (HFSE) show relatively depleted concentrations (Table 2). Chondrite normalized REE patterns for the komatiite and meimechite

(Figure 5) reflect flat LREE patterns and negative Ce anomalies with feeble LREE/HREE ( $\text{La/Yb}_n = 1.03, 0.94$ ), moderate LREE/MREE ( $\text{La/Sm}_n = 1.25, 1.11$ ) and MREE/HREE fractionation ( $\text{Gd/Yb}_n = 0.9, \text{Dy/Yb} = 1.4$ ) trends. Primitive mantle normalized incompatible trace element patterns for the komatiite and meimechite (Figure 5) exhibit pronounced negative anomalies at Nb and Zr-Hf. The low  $(\text{Nb/Th})_{\text{pm}}$  and  $(\text{Nb/La})_{\text{pm}}$  ratios with relatively high  $(\text{La/Nb})_{\text{pm}}$  and  $(\text{Th/Nb})_{\text{pm}}$  for these komatiite and meimechite [ $(\text{Nb/Th})_{\text{pm}} = 0.6, 0.1$ ;  $(\text{Nb/La})_{\text{pm}} = 0.2, 0.1$ ;  $(\text{La/Nb})_{\text{pm}} = 6.2, 11.2$ ;  $(\text{Th/Nb})_{\text{pm}} = 1.7, 13.1$ ] are in agreement with relative LREE enrichment and Nb depletion and higher Th abundances over Nb.

The studied meimechite sample displays higher values for Zr/Hf (39.43) and with lower Zr/Sm (13.15) and Nb/Ta (5.73) values compared to respective primitive mantle values (Zr/Hf = 36, Zr/Sm = 25 and Nb/Ta = 17), while the komatiite shows lower Zr/Hf: 34.5, Zr/Sm: 7.7 and Nb/Ta: 4 with respect to primitive mantle.

#### *Picrobasalt*

Among transition elements, Ni (228 ppm), Cr (866 ppm) and Co (53 ppm) show elevated abundances in the studied picrobasalt, however LILE and HFSE concentrations are relatively depleted (Table 2). Chondrite normalized REE patterns (Figure 5) exhibit flat LREE distributions with negative anomaly at Ce. LREE/HREE ( $\text{La/Yb}_n = 0.74$ ), LREE/MREE ( $\text{La/Sm}_n = 1.02$ ) and MREE/HREE ( $\text{Gd/Yb}_n = 0.84, \text{Dy/Yb} = 0.84$ ) exhibit feeble moderate fractionations. The studied sample displays positive anomalies at Th, La, Ta and negative anomalies at Nb and Zr-Hf on primitive mantle normalized multi-element diagram (Figure 5). The low  $(\text{Nb/Th})_{\text{pm}}$  and  $(\text{Nb/La})_{\text{pm}}$  and relatively high  $(\text{La/Nb})_{\text{pm}}$  and  $(\text{Th/Nb})_{\text{pm}}$  ratios for these rocks [ $(\text{Nb/Th})_{\text{pm}} = 0.44$ ;  $(\text{Nb/La})_{\text{pm}} = 0.2$ ,  $(\text{La/Nb})_{\text{pm}} = 5.33$ ,  $(\text{Th/Nb})_{\text{pm}} = 2.8$ ] are consistent with primitive mantle normalized incompatible trace element abundances reflecting enrichment in LREE with relative depletion in Nb. Zr/Hf (31.9), Zr/Sm (5.46) and Nb/Ta (4.75) ratios are distinctly lower than their primitive mantle counterparts.

#### *High-Mg basalt*

Transitional trace element compositions for high Mg basalt are marked by 422.74 ppm Ni, 661 ppm Cr and 58.22 ppm Co, while LILE and HFSE show relatively depleted concentrations (Table 2). Chondrite normalized REE patterns (Figure 5) exhibit mild LREE and MREE enrichment over HREE with moderately differentiated LREE/HREE ( $\text{La/Yb}_n = 1.8$ ), LREE/MREE ( $\text{La/Sm}_n = 0.9$ ) signatures and prominent MREE/HREE ( $\text{Gd/Yb}_n = 0.84, \text{Dy/Yb} = 0.84$ ) fractionation. Primitive mantle normalized incompatible trace element abundances for the studied high Mg basalt are marked by positive Th, La, Ta anomalies and negative Nb and Zr-Hf anomalies (Figure 5) thereby suggesting distinct LREE enrichment with relative Nb depletion and higher Th and La abundances over Nb. These geochemical

attributes are in conformity with low ( $\text{Nb/Th}_{\text{pm}}=0.14$ ), ( $\text{Nb/La}_{\text{pm}}=0.1$ ) and relatively higher ( $\text{La/Nb}_{\text{pm}}=10.9$ ), ( $\text{Th/La}_{\text{pm}}=0.66$ ) and ( $\text{Th/Nb}_{\text{pm}}=7.2$ ) ratios. The studied samples exhibit higher Zr/Hf (40.7) and lower Zr/Sm (12.14), Nb/Ta (5.03) ratios against respective primitive mantle values.

### *Foidite*

Transitional trace elements display elevated abundances marked by 259-992 ppm Ni, 245-1770 ppm Cr and 57-86 ppm Co. Incompatible trace element chemistry including LILE and HFSE compositions shows depleted concentrations of elements (Table 2). Chondrite normalized REE patterns for the foidites (Figure 5) exhibits variable LREE distributions over over MREE and HREE complemented by feeble to strongly fractionated LREE/MREE and LREE/HREE patterns ( $\text{La/Sm}_n=0.43-1.84$ ,  $\text{La/Yb}_n=0.5-2.3$ ). The studied samples show moderate to pronounced MREE/HREE fractionations ( $\text{Gd/Yb}_n=1.05-1.3$ ;  $\text{Dy/Yb}=1.45-1.85$ ). One sample CG 80/102 shows distinct positive anomalies at Tb and Tm on chondrite normalized REE diagram. Primitive mantle normalized incompatible trace element patterns for foidites (Figure 5) demonstrate distinct positive anomalies at Th, La, Ta and negative anomalies at Nb and Zr-Hf which collectively point towards with enriched LREE compositions with relative Nb depletion and higher Th abundances over Nb. These observations are further supported by low ( $\text{Nb/Th}_{\text{pm}}$ ), ( $\text{Nb/La}_{\text{pm}}$ ) and comparatively higher ( $\text{La/Nb}_{\text{pm}}$ ), ( $\text{Th/La}_{\text{pm}}$ ) and ( $\text{Th/Nb}_{\text{pm}}$ ) ratios for the foidites [ $\text{Nb/Th}_{\text{pm}}=0.12-0.3$ ;  $\text{Nb/La}_{\text{pm}}=0.07-0.08$ ;  $\text{La/Nb}_{\text{pm}}=12.01-14.42$ ;  $\text{Th/La}_{\text{pm}}=0.24-0.66$  and  $\text{Th/Nb}_{\text{pm}}=3.45-8.28$ ] The HFSE chemistry of the samples is characterized by variable Zr/Hf (26.25-42.64), Zr/Nb (18.3-105.2), Zr/Sm (3.9-13.21) and Nb/Ta (1.15-4.1) with respect to primitive mantle values.

### *Basanite*

Among transitional trace elements, basanites are having Ni ranging from 199-261 ppm, Cr varying between 340-416 ppm and Co in the range of 49 to 80 ppm. Incompatible trace element abundances are characterized by depleted concentrations of LILE and HFSE (Table 2). Chondrite normalized REE diagram for basanites (Figure 5) reflect flat REE patterns with feeble to moderate LREE/HREE ( $\text{La/Yb}_n=0.38-1.14$ ), LREE/MREE ( $\text{La/Sm}_n=0.4-1.2$ ) and moderate MREE/HREE fractionation trends ( $\text{Gd/Yb}_n=1-1.3$ ,  $\text{Dy/Yb}=1.5-1.9$ ). One sample CG 80/114 shows distinct positive anomalies at Tb and Tm on chondrite normalized REE diagram. The basanites are characterized by low ( $\text{Nb/Th}_{\text{pm}}=0.1-0.2$ ), ( $\text{Nb/La}_{\text{pm}}=0.1-0.11$ ) and relatively higher ( $\text{La/Nb}_{\text{pm}}=8.96-11.22$ ), ( $\text{Th/La}_{\text{pm}}=0.56-0.94$ ) and ( $\text{Th/Nb}_{\text{pm}}=4.97-10.55$ ) ratios that collectively endorse LREE enrichment with relative Nb depletion and higher Th and La abundances over Nb. These geochemical features are comparable with positive Th, La, Ta anomalies and negative Nb and Zr-Hf anomalies on primitive mantle normalized multi-

element diagram (Figure 5). The studied samples exhibit variable Zr/Hf (24.7-47.8), Zr/Sm (8.72-22.11), Zr/Nb (60.9-160.8) and Nb/Ta (2.2-4.99) ratios with respect to primitive mantle values.

## 6. Discussion

### 6.1 Petrogenesis: Mantle melting, Crustal contamination and Plume-lithosphere interaction

#### 6.1.1 Komatiite-Meimechites

Rare-earth element compositions are sensitive to mantle melting conditions and provide important constraints in understanding the degree and depth of partial melting because their relative abundances in mantle-derived melts are strongly dependent on the extent of partial melting and the nature of aluminous phase (spinel or garnet) in the mantle source (Reichow et al., 2005; He et al., 2010; Manikyamba et al., 2015). Komatiites have been classified as Al-depleted, Al-undepleted, Ti-enriched and Ti-depleted types based on TiO<sub>2</sub> content, CaO/Al<sub>2</sub>O<sub>3</sub>, Al<sub>2</sub>O<sub>3</sub>/TiO<sub>2</sub> and (Gd/Yb)<sub>n</sub> ratios (Hanski et al., 2001; Sproule et al., 2002; Manikyamba et al., 2013; Manikyamba and Saha, 2014b). These compositional variations of komatiites reflect variable source compositions and mantle melting conditions.

Al-undepleted komatiites are interpreted as melts derived by high degree of partial melting of mantle at shallow depth in the stability field of spinel peridotite where garnet enters the melt portion or by high degree, partial melting of a garnet peridotite source at relatively greater depth leaving a garnet-free residue. Al-depleted komatiites were inferred to be derived either from dynamic melting of a refractory source leaving a refractory harzburgite residue, similar to the source of Gorgona picrites, or alternatively, high-degree melting of a garnet peridotite source with garnet as residual phase. Ti-enriched komatiites reflect partial melting of a garnet peridotite source leaving a garnet-bearing residue. The studied Al-undepleted komatiite from ultramafic enclaves of CGG with Al<sub>2</sub>O<sub>3</sub>/TiO<sub>2</sub>=116.22; CaO/Al<sub>2</sub>O<sub>3</sub>=0.6, moderate concentrations of Ni and Cr, flat to moderately fractionated REE patterns coupled with (Gd/Yb)<sub>n</sub> = 0.9 and Dy/Yb=1.4 suggest that the komatiites were derived through higher degree (30%-50%) of partial melting of mantle at a shallower level (~90 km) with garnet free residuum. Dy/Yb vs. La/Yb and Sm/Yb vs. Sm plots (Figures 6A and 6B) suggest derivation of parent melts by higher degree (~30% melting) partial melting of mantle having a spinel peridotite composition. Therefore, the studied Al-undepleted komatiite, like those of Neoproterozoic greenstone belts are geochemically similar to the Munro-type komatiites which were generated by high degree, shallow level partial melting of anhydrous, depleted, hot mantle sources with a garnet free residue. The derivation of parent magma by high degree melting of mantle at shallow depth accounted for elimination of garnet from residue that is reflected in their geochemical signatures. The Al-

undepleted komatiite and meimechite characterized by depleted trace and REE chemistry reflects high degree partial melting of a refractory mantle. The low  $(La/Yb)_n$  and  $(Gd/Yb)_n$  ratios, negative Zr, Hf anomalies on mantle normalized multi-element diagram corroborate high degree (>30%) of mantle melting and suggest derivation of parent magma by melting under anhydrous conditions at shallow mantle domain leaving behind a garnet free residue.

Compositional variations in mantle-derived magmas have been attributed to variable amounts of contamination by different crustal components during their ascent to the surface through continental crust (Mahoney, 1988; Hawkesworth et al., 1984; Song et al., 2008). Trace element compositions provide appropriate geochemical tracers to decipher the open and closed system magmatic processes like crustal assimilation and fractional crystallization (Condie, 2003; Reichow et al., 2005; Shellnutt et al., 2014). Due to their high liquidus temperature, ultramafic melts are susceptible to contamination either through assimilation-fractional crystallization (AFC) or thermal erosion of floor rocks during their ascent and eruption owing to their high liquidus temperature. Conventionally, such contamination has been estimated through AFC modeling with various possible crustal contaminant compositions (Arndt and Jenner, 1986; Huppert and Sparks, 1985; Puchtel et al., 1997, 2007). The Nb/Th ratio of primitive mantle is 8, whereas in continental crust, it is ~1.1 (Rollinson, 2008; Rudnick and Gao, 2003; Sun and McDonough, 1989; Taylor and McLennan, 1985). Evidence of crustal assimilation in the studied komatiite and meimechite has been interpreted in terms of a mantle plume erupted proximal to a rifted craton margin, wherein the values  $Nb/Th > 8$  represent eruption in an oceanic domain while the values  $Nb/Th < 8$  were inherited from eruption through rifted continental crust. Negative Nb anomalies observed for the komatiite and meimechite samples are attributed either to contribution from sub-continental lithospheric mantle or to assimilation of lower crustal materials. Mantle plumes cannot melt beneath thick continental lithosphere, but rather are steered to thinner, rifted, margins where melting is induced by decompression at a depth of ~150 km (Kerrick et al., 2005; Sleep, 2006). The studied samples have Nb/Th ratios ranging from 0.6-4.9 implying assimilation of continental crust. In contrast to the scenario of crustal assimilation, contamination of the studied komatiite and meimechite also invoke a possibility of interaction of mantle plumes with metasomatized continental mantle lithosphere as advocated by their Nb/Th values and recorded for komatiites and associated tholeiitic basalts of the Kalgoorlie terrane (Said and Kerrich, 2010; Said et al., 2010).

The  $K_2O/P_2O_5$  and  $TiO_2/P_2O_5$  ratios for komatiite and meimechite (Table 2) reflect relatively greater assimilation of crustal components by the meimechite. Among subduction-metasomatized mantle lithosphere and crustal contamination processes (Lassiter and DePaolo, 1997), it has been inferred that the former dominated as mantle plumes interacted with the base of the lithosphere. Based

on the same criteria, we conclude that the studied komatiites might have also been contaminated by interaction of a mantle plume with metasomatized continental mantle lithosphere, likely at a rifted craton margin. Both assimilation of older crustal materials and contributions from subduction-modified lithospheric mantle account for negative Nb-Ta anomalies; whereas negative Nb-Ta coupled with positive Zr-Hf anomalies are solely attributed to crustal contamination. In this study the negative Nb-Ta and Zr-Hf anomalies for the komatiite and meimechite imply dominant involvement of subduction-processed sub-continental lithospheric mantle material had its interaction with plume-derived magma as documented from komatiites of Kambalda terrane, Australia. Elevated Zr/Hf ratios of meimechite, in comparison with the primitive mantle ratio of 36, attest to contribution from a metasomatized lithospheric mantle in their genesis. Although the Th–Nb–Zr–Hf systematics suggests contamination by sub-continental lithospheric mantle, contamination by older continental crust cannot be ruled out, given that subduction-modified lithospheric mantle and continental crust have similar trace element characteristics. Thus, subtle contamination of these komatiite and meimechite by older continental crust and prominent interaction between mantle plume and subduction-metasomatized sub-continental lithospheric mantle are inferred.

### **6.1.2 Picrobasalt-high Mg basalt-foiidite-basanite**

The studied alkaline ultramafic volcanic rocks have  $(La/Yb)_n$  ratios (0.46-2.27) that attest to pronounced LREE enrichment with relative depletion in HREE corresponding to low degree melting in a mantle regime having spinel to garnet lherzolitic composition. This proposition indicates that the melting domain extended over a variable depth range from the stability field of spinel to garnet with respective occurrence of spinel and garnet as stable phase in the mantle restite. The  $(La/Sm)_n$  ratios for the studied samples range from 2.7 to 5.7 corroborating LREE enrichment over MREE and are in compliance with the above contention. Partial melting occurring at a sufficient depth for garnet to remain in the source area will elevate the middle to heavy REE ratio (i.e. Dy/Yb, Gd/Yb) in the melt (Lassiter and DePaolo, 1997). Dy/Yb and Gd/Yb are strongly fractionated when melting occurs in the garnet stability field and nearly unfractionated during melting in the spinel peridotite domain (Yaxley, 2000; Xu et al., 2005; Davidson et al., 2013). These attributes have made Dy/Yb and Gd/Yb distinct geochemical indicators of the presence of residual garnet during partial melting and for distinguishing melting between the spinel and garnet stability fields of lherzolitic mantle (Kelemen, 1990; Yang et al., 2014).  $(Gd/Yb)_n > 1$  for the studied samples ( $Gd/Yb_n$ : 0.84-1.92) provides evidence for parent magma generation within the stability field of garnet (Herzberg, 1992) and attests to the involvement of garnet lherzolite mantle in the melting and generation of parent magma. High Dy/Yb ratios ( $>2.5$ ) are ascribed to partial melting in the garnet stability field, while Dy/Yb ratios  $<1.5$  are derived through

melting in the stability field of spinel (Yang et al., 2014).

The studied volcanic rocks are characterized by Dy/Yb ratios ranging from 1.61 to 2.8 implying that the mantle source carried signatures of both spinel and garnet lherzolite and the parental melts were generated by low degree partial melting of garnet–spinel lherzolite transitional field corresponding to depth ranging from 30-90 km. On Dy/Yb vs. La/Yb plot (Figure 6A) the picrobasalt-high Mg basalt-foiidite-basanite samples cluster in the field of spinel-peridotite facies which is indicative of shallow level mantle melting in the stability field of spinel peridotite. Sm/Yb vs Sm variations corroborate variable degrees of partial melting of a spinel lherzolite mantle (Figure 6B); however the foidite-basanite and picro basalt-high Mg basalt samples correspond to distinctly lower and higher degrees of melting respectively.

The alkaline ultramafic have high  $K_2O/P_2O_5$  ( $>2$ ) in the range of 2-53. This feature indicates prominent involvement of silicic crustal component from older sialic basement or wall rock (of granitic composition) assimilation during their ascent. The  $TiO_2/P_2O_5$  ratios for these rocks suggest that the parental melts were affected by contamination from granitic continental crust (Carlson and Hart, 1988). The La/Nb ratios (5.14-13.90) of the studied samples reflect crustal contamination of parent magma (Peate et al., 1999; Song et al., 2001). HFSE ratios are suitable indicators of crustal contamination in an open magma system. The Nb/Th ratio of primitive mantle is 8, whereas in continental crust it is  $\sim 1.1$  (Taylor and McLennan, 1985; Sun and McDonough, 1989; Rudnick and Gao, 2003). The studied samples characteristically have Nb/Th ratios varying between 1.01 and 2.43 which indicate contribution from continental crust. The studied rocks have relatively higher Zr/Nb and Th/Nb ratios (and respectively) than those of OIB (4.2 and 0.06 respectively; Hoffmann, 1997; Ionov et al., 1997) conforming to the possibility of contamination from older continental crustal materials. Low  $(Nb/La)_{pm}$  values are attributed to either exogenous contamination of ascending melts by continental crust or endogeneous contamination through recycling of subducted oceanic lithosphere into the mantle (Mahoney et al., 1993; Hofmann, 1997; Polat et al., 1999; Simonov et al., 2014). The low Nb contents,  $(Nb/La)_{pm}$  and  $(Nb/Th)_{pm}$  ratios in combination with high Th concentrations, Th/Ta, Th/Ce,  $(Th/La)_{pm}$ , and  $(Th/Nb)_{pm}$  ratios for the volcanic rocks under study can be accounted in terms of both endogeneous and exogenous contamination of parental melts.

## **6.2 Mantle source characteristics**

### **6.2.1 Komatiite and Meimechite**

HFSE and REE, being resistant to alteration, serve as useful geochemical proxies to distinguish different possible melt sources for mantle-derived magmas (Le Roex et al., 1983). Pearce (2008)

suggested that HFSE ratios involving Nb, Th, Yb provide significant constraints on the mantle components in the genesis of mafic-ultramafic volcanic rocks at different tectonic settings. High pressure experimental studies show that komatiitic melts can be produced by low degree of mantle melting at high pressure (greater depth) or higher degree of mantle melting at lower pressure (shallow level) (Arndt, 2003; Herzberg, 1992;). Nb-Th-Yb can be used as effective geochemical proxies to understand relative mantle, subduction and crustal inputs in magma genesis. Pearce (1982, 2008) developed Th/Yb versus Nb/Yb and Ta/Yb plot that distinguishes arc and non-arc mantle sources and discriminates convergent margin magmas from that of within-plate and spreading centers. The mantle array extends from normal mid-ocean ridge basalts (N-MORB) through enriched mid-ocean ridge basalts (E-MORB) to alkaline ocean island basalts (OIB). The studied komatiite and meimechite plot away from the MORB-OIB array on Th/Yb vs. Nb/Yb plot (Figure 7A) thereby indicating role of lithospheric mantle lithosphere containing an inherited subduction component. These rocks are depleted in LILE and LREE relative to moderately incompatible elements like Zr, Hf, Ti, HREE indicating that they were derived from sources with depletion of these elements. Zr/Hf, Zr/Sm and Nb/Ta values for komatiite and meimechite (Table 2) in comparison with primitive mantle (Zr/Hf: 36, Zr/Sm; 25 and Nb/Ta: 17) suggest a depleted mantle source for their origin. The existence of an intrinsic depleted component in mantle plumes is ascribed to multistage melting at plume initiation, where depleted melts reflect entrainment and melting of depleted upper mantle (Buchs et al., 2016). CaO/Al<sub>2</sub>O<sub>3</sub>, Al<sub>2</sub>O<sub>3</sub>/TiO<sub>2</sub> and Gd/Yb<sub>n</sub> ratios serve as effective geochemical parameters to evaluate mantle source characteristics in terms of garnet dissolution, fractionation or retention of garnet in the mantle residue (Jahn et al., 1982; Chavagnac, 2004; Jayananda et al., 2008). Gd/Yb<sub>n</sub> vs. Al<sub>2</sub>O<sub>3</sub>/TiO<sub>2</sub> plot (Figure 7B) for the studied Al-undepleted komatiite and meimechite samples conform to parent magma origin from a relatively shallow plume source by high-degree partial melting. The geochemical attributes of the studied LREE-depleted komatiite and meimechite corroborate their origin from hot, depleted mantle plume sampling variably depleted mantle asthenosphere with the parent melts steering towards craton margin and erupting through thinned and rifted continental lithosphere. The geochemical signatures of the studied komatiite and meimechite marked by low Nb/La<sub>pm</sub> with relatively higher Th/Nb<sub>pm</sub> values attest to their derivation from ultramafic melts of a depleted plume source that assimilated subduction-derived components (SDC) components of lithospheric mantle. The higher Zr/Hf values for meimechite as compared to primitive mantle and the studied komatiite indicate metasomatic enrichment of parent melt.

### **6.2.2 Picrobasalt-high Mg basalt-foiidite-basanite**

Geochemical and isotopic studies of silica-undersaturated alkaline magmas of basanite-foiidite



compositional varieties invoke distinct mantle sources for their generation including an enriched, asthenospheric plume-type source, a depleted mantle source located in the lithospheric mantle or upper most asthenosphere and a veined lithospheric mantle source (Niu et al., 2012). The studied samples have Nb (0.12-0.45 ppm) and Zr (2.68-41.25 ppm) contents lower than those of the N-MORB (Nb=2.33 ppm, Zr =74 ppm) implying their generation from a depleted mantle source (Sun and McDonough, 1989). The picrobasalt-high Mg basalt-foiidite-basanite from the study display higher Zr/Hf with lower Zr/Sm and Nb/Ta values compared to primitive mantle (Zr/Hf=36, Nb/Ta=17 and Zr/Sm=25; Menzies et al., 1991). The conjunction of low Nb/Ta and Zr/Sm values with high Zr/Hf ratios is consistent with melting of amphibole bearing veins in a metasomatized lithospheric mantle source with rutile as residual phase. Pearce and Norry (1979) and Le Roex *et al.* (1983) have emphasized the importance of Zr/Nb ratio as indicator of the 'depleted' or 'enriched' nature of the source region for basaltic magmas. The Zr/Nb ratios of the investigated samples including all the compositional varieties range from 11.7 to 35.9 showing lower values in comparison to N-MORB (Zr/Nb: >301). This feature suggests that the parental melts for the studied rocks (excluding komatiite and meimechite) were derived through partial melting of a mantle enriched by metasomatized lithospheric components. Th/Yb vs. Nb/Yb plots (Figure 7A) for these rocks attest to melt-lithosphere interaction and substantiates their origin from a heterogeneous mantle source not associated with any active subduction processes, involving plume-derived asthenospheric melts and metasomatized lithospheric components. The plots of studied samples in Gd/Yb<sub>n</sub> vs. Al<sub>2</sub>O<sub>3</sub>/TiO<sub>2</sub> diagram (Figure 7B) corroborate the role of a mantle source carrying depleted and enriched components. Zr/Ba ratio can be considered as an effective parameter to distinguish lithospheric sources (Zr/Ba: 0.3-0.5) from asthenospheric sources of parent melt (Zr/Ba: >0.5) (Menzies et al., 1991; Kürkcüoğlu, 2010). In the present scenario, the Zr/Ba ratio of the studied samples ranging from 0.08 to 0.6 indicates minor involvement of depleted asthenospheric mantle source of MORB affinity in the melting process. Condie (2003, 2005) applied Nb/Th vs. Zr/Nb variations in order to advocate three mantle domains viz. enriched mantle (EM), depleted mantle (DM), and hydrated mantle (HM) for origin of basaltic magmas covering a time span ≥2200 Ma-<1000 Ma. EM consists of high Nb/Th ratios but Zr/Nb ratios restricted to < 20. DM is characterized by Th and Nb depletion relative to Nb and Zr respectively thereby showing high values of Nb/Th (> 8) and Zr/Nb (> 20), whereas HM is marked by very low Nb/Th (<8) and variable Zr/Nb ratios (Condie, 2015). On Zr/Nb vs. Nb/Th plot (Figure 7C), the studied volcanic rocks occupy the field of hydrated mantle. In summary, the geochemical characteristics indicate (i) magmatism controlled by mantle metasomatism, mixing between depleted and enriched mantle components, crustal recycling/assimilation and (ii) volatile induced partial melting of mantle at variable pressure-temperature conditions and under compressional-extensional stress regime that

results into magmas of tholeiitic, calc-alkaline and alkaline compositions.

In terms of Th-Nb-LREE compositions, the studied volcanic rocks with high Ce/Nb and low Th/Nb reflect the involvement of depleted mantle (DM) in their genesis (Safonova, 2009; Saunders et al., 1988; Safonova et al., 2008). However, the low Nb/La<sub>pm</sub> and relatively high Th/Nb<sub>pm</sub> ratios attest to contributions from subduction-derived component (SDC) in the melting process. These observations collectively suggest that parental melts for the studied volcanic rocks were derived from a chemically heterogeneous lithospheric mantle source that experienced extensive interaction between plume-related depleted mantle (DM) and enriched subduction-derived components (SDC).

### **6.3 Tectonic Implications: plume-craton interaction and continental lithospheric evolution**

Continents formed by combinations of magmatic, metamorphic and tectonic processes and two distinct modes have been recognized for continental growth (Touret et al., 2016). Lateral growth of continents occurs above oceanic subduction zones by top-down magmatic processes in a high pressure metamorphic regime while vertical growth of continents invoke accumulation of mantle derived magmas at the base of the crust by bottom up process in a high temperature metamorphic regime.

Oceanic plateau and intraoceanic arc sequences from Archean greenstone terranes involve a complex magmatic history with heterogeneous mantle and crustal sources, evolution of microplates, episodic subduction processes, plume-arc accretion all collectively contributing to lithospheric mantle evolution (Naqvi et al., 1988; Wyman and Kerrich, 2009). Compositionally diverse magmatic units from both convergent margin and intraplate settings are present. The former include boninite, through low-, medium-, and high-K basalts to shoshonite and leucitite association, and the adakite-Mg andesite-Nb enriched basalt association, as in Phanerozoic arcs (Stern et al., 1995). The latter include intra-oceanic plume-derived associated komatiites-tholeiites, high-Mg, and alkaline basalts. Collectively, these diverse lithological associations, were accreted and preserved in Archean greenstone terranes (Naqvi et al., 2002; Naqvi et al., 2006; Hollings and Kerrich, 2006). Archean komatiite-komatiitic basalt sequences are erupted in intra-oceanic settings as oceanic plateaus and through continents as continental flood basalts provinces (Kerrich and Polat, 2006). The 3.51 to 3.2 Ga basalt succession of the Pilbara craton erupted as intra-oceanic plateau with younger equivalents erupted through 3.5 Ga continental crust (Arndt et al., 2005). The 3.0 Ga North Caribou greenstone belt in the Superior Province preserves a komatiite-basalt sequence which records pristine plume melts and crustally contaminated equivalents, interpreted as plume impingement at a rifted craton margin (Hollings and Kerrich, 1999; Said and Kerrich, 2010). Plume-craton interaction at a rifted, thinned craton margin has also been proposed for the contaminated and uncontaminated komatiite-basalt

sequence of Kambalda, specifically by interaction of mantle plumes with metasomatized continental mantle lithosphere (Said and Kerrich, 2010; Said et al., 2010).

A careful study of the tectonic evolution of the region suggests that towards the end of the Archean time, a series of elongated troughs developed around stabilized Singhbhum Craton composed essentially of Older Metamorphics, Iron Ore Group of rocks and Singhbhum granite batholith. The CGG is correlatable with the Singhbhum granite (SBG) phase III (3.12 Ga; Table 1) with portions that may represent Older Metamorphic Tonalite Gneiss of the type area (Saha, 1994; Sharma, 2009; Sarkar and Saha, 1964; Bandopadhyay and Sengupta, 1984; Sengupta et al., 1991). The emplacement of Chakradharpur granite complex might have taken place along the western margin of the deep seated suture (shear zone) that straddles the Singhbhum craton during the waning phase of Iron Ore Orogeny. The closing of Iron Ore Group sedimentation in this part of the area is marked by deposition of a thick sequence of arkose-conglomerates near the interface or base of the younger Singhbhum Group of rocks (late Paleoproterozoic Chaibasa Formation, Mazumder, 2003; 2005). While some of the enclaves of the low-grade schists in CGG might represent the older Iron Ore Group sediments, the arkose-conglomerate enclaves may represent younger cover sediments that have been pinched into sharp synforms in the process of regional folding ( $F_1$  and  $F_2$ ). In comparison with the Dalma greenstone belt of the SMB to its west (Figure 1), the western part of the Chakradharpur granite appears to occupy the antiformal core.

In this study, the komatiite, microbasalt, high-Mg basalt, foidite and basanite enclaves preserved in Chakradharpur granite gneisses are analogous to an Archean greenstone belt association originating from plume-lithosphere magmatism at a rifted cratonic margin. This conjecture provides insights into the evolution of Archean mantle-lithosphere system of the Singhbhum Craton. The ancient, stable nucleus of continents is sometimes underlain by keels of deep lithospheric roots that form distinct features of Archean cratons (Eaton and Claire Perry, 2013). These cratonic keels deflect the melts derived by decompression melting of an ascending plume and channel them towards the edge of the continent (Sleep et al., 2002). The genesis of komatiites of the study area is envisaged in terms of deflection of plume-derived melts towards cratonic margin and their eruption through rifting of thinned lithosphere. The base of the lithosphere offers a potential site for incubation of an upwelling mantle plume (Wyman, 2013). The lithosphere formed in Archean-Paleoproterozoic times was thicker, buoyant and geochemically distinct from post 2.3 Ga lithosphere, however underwent interactions with hot asthenospheric melts from an upwelling mantle plume that supplied heat to the base of the lithosphere, induced melting, thermal erosion and entrainment of lithospheric mantle melts into the asthenospheric flow (Sleep et al., 2002). The origin of ultramafic-mafic magmas of alkaline chemistry in an intraplate

continental setting, as observed in the studied lithologies (microbasalt-high Mg basalt-foiidite-basanite), has been advocated in terms of melting of a metasomatized sub-continental lithospheric mantle (SCLM) carrying subduction derived components. The metasomatism of mantle lithosphere beneath oceans or continents can be attributed to the occurrence of hydrous minerals e.g. amphibole, phlogopite and veined lithologies comprising pyroxenite, hornblendite, garnet pyroxenite (Niu et al., 2012). These metasomatic agents modify the SCLM and induce incipient partial melting in the presence of CO<sub>2</sub> and H<sub>2</sub>O. The plume melts ascending through the SCLM assimilate the metasomatic veins. Geochemical signatures of the studied lithologies with subalkaline and alkaline compositions endorse two distinct melt sources and discrete melting episodes during plume-lithosphere interaction for the generation of komatiite-meimechites and microbasalt-high Mg basalt-foiidite-basanite suite. In the first magmatic episode, komatiite-meimechite were derived by high degree shallow level melting of plume materials deflected and channeled towards thinned lithosphere beneath rifted craton margin. The latter stage involved assimilation of metasomatic components of SCLM by ascending melts of plume incubating at the base of lithosphere, variable extents of melting at different depths and melt generation. The possible geodynamic model (Figure 8) that accounts for the compositional diversity of the studied volcanic rocks invokes (i) impingement of mantle plume at the base of SCLM beneath the Singhbhum craton (ii) mantle melting at different depths during plume ascent through lithosphere beneath rifted craton margin (iii) higher degrees of partial melting in the plume head at <90 km produced the komatiites at the rifted edge of continent (iv) picrites, high Mg-basalts, foidites and basanite were derived by plume-lithosphere interaction towards continental core, higher degrees of melting at relatively shallower depth produced microbasalt and high Mg basalts, while lower degree melting at deeper level generated ultramafic alkaline magmas. Plume impingement at a rifted, thinned craton margin and melting of metasomatized SCLM triggered by heat from an upwelling plume collectively contributed to the ultramafic, mafic and alkaline magmatism, addition of crustal materials and continental lithospheric evolution in the study area.

## 7. Conclusions

- The Chakradharpur Granite Gneiss (CGG) from the Singhbhum Craton of the eastern Indian shield, equivalent to the 3.12 Ga Singhbhum Granite (SBG) phase III, hosts numerous enclaves or rafts of tonalitic gneisses, metamorphosed ultramafic-mafic volcanics, metasediments and conglomerates that collectively represent vestiges of an older (Paleoarchean) greenstone belt.
- The ultramafic enclaves are characterized by greenschist facies metamorphism represented by atalc-chlorite-tremolite assemblage with development of pressure solution and

crenulation cleavages prominent development of schistosity.

- Geochemical attributes classify the ultramafic volcanic enclaves as komatiite-meimechite and picrobasalt-highMg basalt-foiidite-basanite representing subalkaline and alkaline compositional varieties.
- The melts parental to komatiite-meimechite were (i) derived by high degree (~50%), shallow level (<90 km) partial melting of a hot, anhydrous, mantle plume, carrying depleted components (ii) deflected by Archean cratonic keels (iii) channeled towards cratonic margin and (iv) erupted through rifted, thinned continental lithosphere.
- These komatiite-meimechite preserve evidence for interaction between metasomatized sub-continental lithospheric mantle (SCLM) and asthenospheric melts from a plume impregnating at the base of continental lithosphere.
- Picrobasalt-highMgbasalt-foiidite-basanite rocks originated from polybaric melting of a chemically heterogeneous, lithospheric mantle source comprising depleted and enriched components inherited from gestating mantle plume and metasomatized sub-continental lithospheric mantle.
- Parental melts for ultramafic alkaline melts were generated through partial melting of metasomatized sub-continental lithospheric mantle triggered by heat transfer from impinging mantle plume. Picrobasalt and high-Mg basalts were produced by higher degrees of melting at relatively shallower depth (spinel peridotite), while ultramafic alkaline magmas were derived by lower degree melting at deeper level (garnet peridotite).
- The ultramafic enclaves of CGG representing vestiges of Archean greenstone in the Singhbhum Craton of eastern Indian shield margin, reflect crustal growth and lithospheric evolution through plume-craton interaction, two distinct melting episodes and magmatism operative at thinned craton margins and rifted continental interior.

## **Acknowledgments**

The authors are thankful to Nilanjan Chatterjee, MIT, Cambridge, Boston for critical comments and suggestions on an earlier version of the manuscript. AS expresses his gratitude to the Director, CSIR-National Institute of Oceanography and Head, Geological Oceanography Division, CSIR-National Institute of Oceanography, Goa for their encouragement and permission to publish this work. The authors thank the handling Associate Editor and two reviewers for their insightful suggestions which have greatly improved the quality of the manuscript. Drs. A.Keshav Krishna and M.Satyanarayanan,

CSIR-National Geophysical Research Laboratory, Hyderabad are thankfully acknowledged for providing the XRF and HR-ICP-MS data. M.M. Korkoppa of the Geological Survey of India, Bangalore for EPMA at the PPOD Laboratory are gratefully acknowledged. This is NIO's contribution No. XXXX.

## References

- Acharyya, S.K., Gupta, A., Orihashi, Y., 2010a.** New U-Pb zircon ages from Paleo-Mesoarchean TTG gneisses of the Singhbhum Craton, Eastern India. *Geochemical Journal* **44**, 81-88.
- Acharyya, S.K., Gupta, A., Orihashi, Y., 2010b.** Neoproterozoic–Paleoproterozoic stratigraphy of the Dhanjori basin, Singhbhum Craton, Eastern India: And recording of a few U–Pb zircon dates from its basal part. *Journal of Asian Earth Sciences* **39**, 527-536.
- Ahmad, T., Deb, M., Tarney, J., Raza, M. 2008.** Proterozoic mafic volcanism in the Aravalli- Delhi Orogen, North-western India: geochemistry and tectonic framework. *Journal of Geological Society of India* **72**, 93–111.
- Aldanmaz, E., Pearce, J.A., Thirlwall, M.F., Mitchell, J.G. 2000.** Petrogenetic evolution of late Cenozoic, post-collision volcanism in western Anatolia, Turkey. *Journal of Volcanological and Geothermal Research* **102**, 67–95.
- Arndt, N. 2003.** Komatiites, kimberlites and boninites. *J. Geophys. Res.* **108**, 2293-2304.
- Arndt, N. T., Jenner, G. A. 1986.** Crustally contaminated komatiites and basalts from Kambalda, Western Australia. *Chemical Geology* **56**, 229-255
- Arndt, N., Nisbet, E.G. 1982.** Komatiites. Allen and Unwin, London.
- Arndt, N.T., C.M. Lesher C.M., Czamanske, G.K. 2005.** Mantle-derived magmas and magmatic Ni-Cu-(PGE) deposits. *Economic Geology, 100th Anniversary volume*, 5-24.
- Bandyopadhyay, P. K. 1981.** Chakradharpur Granite Gneiss—a composite batholith in the western part of the Singhbhum shear zone, Bihar. *Indian Journal of Earth Sciences* **8**, 109-118.
- Bandyopadhyay, P. K. 1983.** Some geochemical characteristics of the Chakradharpur granite gneiss body in West Singhbhum and their bearing on its evolution. *Quarterly Journal of the Geological Mining and Metallurgical Society of India* **65**, 137-147.
- Bandyopadhyay, P. K., Sengupta, S. 1984.** The Chakradharpur granite gneiss complex of west Singhbhum, Bihar. *Monograph of Crustal Evolution*, 75-90.
- Barnes, S.J., Van Kranendonk, M.J. 2014.** Archean andesites in the east Yilgarn craton, Australia: products of plume-crust interaction? *Lithosphere* **6**, 80-92.
- Basu, A.R., Ray, S.L., Saha, A.K., Sarkar, S.N. 1981.** Eastern Indian 3800 Million year-old crust and mantle differentiation. *Science* **212**, 1502-1506.

- Bedard, J.H. 2018.** Stagnant lids and mantle overturns: Implications for Archean tectonics, magmagenesis, crustal growth, mantle evolution and the start of plate tectonics. *Geoscience Frontiers* **9**, 19-40.
- Bose, M.K. 2009.** Precambrian mafic magmatism in the Singhbhum Craton, eastern India. *Journal of the Geological Society of India* **73**, 13-35.
- Buchs, D.M., Hoernle, K., Hauff, F., Baumgartner, P.O., 2016.** Evidence from accreted seamounts for a depleted component in the early Galapagos plume. *Geology* **44**. 383-386.
- Campbell, I.H., Griffiths, R.W. 1990.** Implications of mantle plume structure for the evolution of flood basalts. *Earth Planet. Sci. Lett.* **99**, 79–93.
- Carlson, R.W., Hart, W.K. 1988.** Flood Basalt Volcanism in the Northwestern United States. In: Macdougall, J. D. (Ed.), *Continental Flood Basalts*, Kluwer Academic Publication, Dordrecht, 35-61.
- Chavagnac, V. 2004.** A geochemical and Nd isotopic study of Barberton komatiites (South Africa): implications for the Archean mantle. *Lithos* **75**, 253-281.
- Condie, K. C. 1999.** Mafic crustal xenoliths and the origin of the lower continental crust. *Lithos* **46**, 95-101.
- Condie, K.C. 2003.** Incompatible element ratios in oceanic basalts and komatiites: tracking deep mantle sources and continental growth rates with time. *Geochemistry, Geophysics and Geosystems* **4**, 2002GC000333.
- Condie, K.C. 2005.** TTG and adakites: are they both slab melts? *Lithos* **80**, 33-44.
- Condie, K. C. 2015.** Changing tectonic settings through time: indiscriminate use of geochemical discriminant diagrams. *Precambrian Research* **266**, 587-591.
- Condie, K.C., Kröner, A. 2013.** The building blocks of continental crust: Evidence for a major change in the tectonic setting of continental growth at the end of the Archean. *Gondwana Research* **23**, 394-402.
- Davidson, J., Turner, S., Plank, T. 2013.** Dy/Dy\*: variations arising from mantle sources and petrogenetic processes. *Journal of Petrology* **54**, 525-537
- Dostal, J., Mueller, W.U. 2013.** Deciphering an Archean mantle plume: Abitibi greenstone belt, Canada. *Gondwana Research* **23**, 493-505.
- Dunn, J. A., Dey, A. K. 1942.** The geology and petrology of eastern Singhbhum and surrounding areas. *Government of India Press*, **69**.
- Eaton, D. W., Perry, H. C. 2013.** Ephemeral isopycnicity of cratonic mantle keels. *Nature Geoscience* **6**, 967-970.
- Furnes, H., de Wit, M., Robins, B. 2013.** A review of new interpretations of the tectonostratigraphy, geochemistry and evolution of the Onverwacht Suite, Barberton Greenstone Belt, South Africa. *Gondwana Research* **23**, 403-428.

- Ganguly, S., Yang, Q.Y. 2018.** Greenstone belts and their mineral endowment: Preface. *Geoscience Frontiers*. <https://doi.org/10.1016/j.gsf.2017.11.001>
- Ghose, N.C., Basu, A., Bhaumik, N., Sharan, A.K. 1984.** Petrography and chemistry of the enclaves within the Chakradharpur granite and their significance in the crustal evolution of the Singhbhum craton, Eastern India. *Indian Journal of Earth Sciences*, CEISM Seminar Volume, Calcutta, pp.50-63.
- Hanski, E., Huhma, H., Rastas, P., Kamenetsky, V.S. 2001.** The Palaeoproterozoic komatiite-picrite association of Finnish Lapland. *Journal of Petrology* **42**, 855-876.
- Hawkesworth, C.J., Rogers, N.W., Vancalsteren, P.W.C. 1984.** Mantle enrichment processes. *Nature* **311**, 331-335.
- He, Q., Xiao, L., Balta, B., Gao, R., Chen, J. 2010.** Variety and complexity of the late Permian Emeishan basalts: reappraisal of plume-lithosphere interaction process. *Lithos* **119**, 91-107.
- Herzberg, C. 1992.** Depth and degree of melting of komatiites. *Journal of Geophysical Research* **97**, 4521-4540.
- Hofmann, A. W. 1997.** Mantle geochemistry: the message from oceanic volcanism. *Nature* **385**, 219.
- Hollings P., Kerrich, R. 2006.** Light earth element depleted to enriched basaltic flows from 2.8 to 2.7 Ga greenstone belts of the Ucgi Subprovince, Ontario, Canada. *Chemical Geology* **227**, 133-153.
- Hollings, P., Kerrich, R. 1999.** Trace element systematics of ultramafic and mafic volcanic rocks from the 3 Ga North Caribou greenstone belt, northwestern Superior Province. *Precambrian Research* **93**, 257-279.
- Huppert, H. E., Sparks, R. S. J. 1985.** Komatiites I: Eruption and flow. *Journal of Petrology* **263**, 694-725.
- Ionov, D.A., Griffin, W.L., O'Reilly, S.Y. 1997.** Volatile-bearing minerals and lithophile trace elements in the upper mantle. *Chemical Geology* **141**, 153-184.
- Jahn, B.-M., Gruau, G., Glikson, A.Y. 1982.** Komatiites of the Onverwacht group South Africa: REE geochemistry Sm/Nd age and mantle evolution. *Contributions to Mineralogy and Petrology* **80**, 25-40.
- Jayananda, M., Kano, T., Peucat, J.-J., Channabasappa, S. 2008.** 3.35 Ga komatiite volcanism in the western Dharwar craton, southern India: Constraints from Nd isotopes and whole-rock geochemistry. *Precambrian Research* **162**, 160-179.
- Kamber, B. S. 2015.** The evolving nature of terrestrial crust from the Hadean, through the Archaean, into the Proterozoic. *Precambrian Research* **258**, 48-82.
- Kelemen, P. 1990.** Reaction between ultramafic rock and fractionating basaltic liquid I. Phase relations, the origin of calc-alkaline magma series, and the formation of discordant dunite. *Journal of Petrology* **31**, 51-98.
- Kerrich, R., Goldfarb, R., Richard, J.P. 2005.** Metallogenic Provinces in an evolving geodynamic framework. *Economic Geology* **100**, 1097-1136.



- Kerrick, R., Polat, A. 2006.** Archean greenstone-tonalite duality: Thermochemical mantle convection models or plate tectonics in the early Earth global dynamics?. *Tectonophysics* **415**, 141-165.
- Kerrick, R., Polat, A., Wyman, D., Hollings, P. 1999.** Trace element systematics of Mg-, to Fe-tholeiitic basalt suites of the Superior Province: implications for Archean mantle reservoirs and greenstone belt genesis. *Lithos* **46**, 163-187.
- Kinzler, R.J. 1997.** Melting of mantle peridotite at pressures approaching the spinel to garnet transition: application to midocean ridge basalt petrogenesis. *Journal of Geophysical Research* **102**, 853-874.
- Krishna, A.K., Murthy, N.N., Govil, P.K. 2007.** Multielement Analysis of Soils by Wavelength-Dispersive X-ray Fluorescence Spectrometry. *Atomic Spectrometry* **28**, 202-212.
- Kürkcüoğlu, B. 2010.** Geochemistry and Petrogenesis of basaltic rocks from the Develidağ volcanic complex, Central Anatolia, Turkey. *Journal of Asian Earth Sciences* **37**, 42-51.
- Kusky, T.M., Polat, A. 1999.** Growth of granite-greenstone terranes at convergent margins and stabilization of Archean cratons. *Tectonophysics* **305**, 43-73.
- Lassiter, J.C., DePaolo, D.J. 1997.** Plume/lithosphere interaction in the generation of continental and oceanic flood basalts: chemical and isotopic constraints. In: J.-J. Mahoney, M. Coffin, (Eds.), Large Igneous Provinces: continental, oceanic and planetary volcanism. American Geophysical Union Monograph Series, 335-355.
- Le Bas, M. J. 2000.** IUGS reclassification of the high-Mg and picritic volcanic rocks. *Journal of Petrology* **41**, 1467-1470.
- Le Roex, A. P., Dick, H. J. B., Erlank, A. J., Reid, A. M., Frey, F. A., Hart, S. R. 1983.** Geochemistry, mineralogy and petrogenesis of lavas erupted along the Southwest Indian Ridge between the Bouvet Triple Junction and 11 degrees east. *Journal of Petrology* **24**, 267-318.
- Mahoney, J.J. 1988.** Deccan Traps. In: Macdougall, J.D. (Ed.) Continental Flood Basalts: Dordrecht, Kluwer, pp.151-194.
- Mahoney, J.J., Storey, M., Duncan, R.A., Spencer, K.J., Pringle, M. 1993.** Geochemistry and geochronology of Leg 130 basement lavas: nature and origin of the Ontong Java Plateau. *Proceedings of the Ocean Drilling Programme, Scientific Results* **130**, 3-22.
- Manikyamba C., Ganguly, S. Santosh, M., Subramanyam, K.S.V. 2017** Volcano-sedimentary and metallogenic records of the Dharwar greenstone terranes, India: Window to Archean plate tectonics, continent growth, and mineral endowment. *Gondwana Research* **50**, 38-66.
- Manikyamba, C., Kerrich, R. 2012.** Eastern Dharwar Craton, India: Continental lithosphere growth by accretion of diverse plume and arc terranes. *Geoscience Frontiers* **3**, 225-240.
- Manikyamba, C., Kerrich, R., Polat, A., Saha, A. 2013.** Geochemistry of two stratigraphically-related ultramafic (komatiite) layers from the Neoproterozoic Sigegudda greenstone terrane, Western Dharwar Craton, India: evidence for compositional diversity in Archean mantle plumes. *Lithos* **177**, 120-135.

- Manikyamba, C., Naqvi, S.M., Rao, D.V.S., Mohan, M.R., Khanna, T.C., Rao, T.G., Reddy, G.L.N. 2005.** Boninites from the Neoproterozoic Gadwal greenstone belt, eastern Dharwar Craton, India: implications for Archean subduction processes. *Earth and Planetary Science Letters* **230**, 65-83.
- Manikyamba, C., Ray, J., Ganguly, S., Singh, M. R., Santosh, M., Saha, A., Satyanarayanan, M. 2015.** Boninitic metavolcanic rocks and island arc tholeiites from the Older Metamorphic Group (OMG) of Singhbhum Craton, eastern India: geochemical evidence for Archean subduction processes. *Precambrian Research* **271**, 138-159.
- Manikyamba, C., Saha A. 2014b.** PGE geochemistry of komatiites from Neoproterozoic Sigegudda greenstone terrane, western Dharwar Craton, India. *Geol. Soc. India, Special Publ.* **2**, 162-174.
- Manikyamba, C., Saha, A., Santosh, M., Ganguly, S., Singh, M. R., Subba Rao, D.V. 2014a** Neoproterozoic felsic volcanic rocks from the Shimoga greenstone belt, Dharwar Craton, India: geochemical fingerprints of crustal growth at an active continental margin. *Precambrian Research* **252**, 1-21.
- Mazumder, R. 2003.** Correlations between the Eastern Block of the North China craton and the South Indian Block of the Indian Shield: an Archean to Palaeoproterozoic link. *Precambrian Research* **127**, 379-380
- Mazumder, R. 2005.** Proterozoic sedimentation and volcanism in the Singhbhum crustal province, India and their implications. *Sedimentary Geology* **176**, 167-193
- Menzies, M.A., Kyle, P.R., Jones, M., Ingram, G. 1991.** Enriched and depleted source components for tholeiitic and alkaline lavas from Zuni-Bandera, New Mexico: inferences about intraplate processes and stratified lithosphere. *Journal of Geophysical Research* **96**, 13645-13671.
- Misra, S. 2006.** Precambrian chronostratigraphic growth of Singhbhum-Orissa Craton, Eastern Indian Shield: an alternative model. *Journal of the Geological Society of India* **67**, 356-378.
- Misra, S., Johnson, P.T. 2005.** Geochronological constraints on the evolution of the Singhbhum Mobile Belt and associated basic volcanics of eastern Indian shield. *Gondwana Research* **8**, 129-142.
- Mohanty, S. 2012.** Spatio-temporal evolution of the Satpura Mountain Belt of India: A comparison with the Capricorn Orogen of Western Australia and implication for evolution of the supercontinent Columbia. *Geoscience Frontiers* **3**, 241-267.
- Moorbath, S., Taylor, P.N., Jones, N.W., 1986.** Dating the oldest terrestrial rocks: facts and fiction. *Chemical Geology* **57**, 63-86.
- Mukhopadhyay, D. 2001.** The Archean nucleus of Singhbhum: the present state of knowledge. *Gondwana Research* **4**, 307-318.
- Mukhopadhyay, J., Beukes, N.J., Armstrong, R.A., Zimmermann, U., Ghosh, G., Medda, R.A. 2008.** Dating the oldest greenstone in India: a 3.51-Ga precise U-Pb SHRIMP zircon age for dacitic lava of the Southern Iron Ore Group, Singhbhum Craton. *Journal of Geology* **116**, 449-461.
- Naqvi, S.M., Khan, R.M.K., Manikyamba, R.M.K., Ram Mohan, C., Khanna, M.T.C. 2006.** Geochemistry of the Neoproterozoic Island Arc Volcanism from Hungund Terrain of Eastern

Dharwar Craton. *J. Asian Earth Sci.* **27**, 25–44.

- Naqvi, S.M., Manikyamba, C., Rao, G., Subba Rao, D.V., Ram Mohan, M., Sarma, S. 2002.** Geochemical and isotopic constraints on Neoproterozoic fossil plumes for the formation of volcanic rocks of Sandur Greenstone Belt, India. *Journal of the Geological Society of India* **60**, 27–56.
- Naqvi, S.M., Rogers, J.J.W. 1987.** Precambrian Geology of India. Oxford University Press, New York, 223 pp.
- Naqvi, S.M., Sawkar, R.H., Subba Rao, D.V., Govil, P.K., Gnaneshwar Rao, T. 1988.** Geology and geochemistry and tectonic setting of Archean graywackes from Karnataka Nucleus, India. *Precambrian Research* **39**, 193-216.
- Nelson, D. R., Bhattacharya, H. N., Thern, E. R., Altermann, W. 2014.** Geochemical and ion-microprobe U–Pb zircon constraints on the Archean evolution of Singhbhum Craton, eastern India. *Precambrian Research* **255**, 412-432.
- Niu, Y., Wilson, M., Humphreys, E. R., O'Hara, M. J. 2012.** A trace element perspective on the source of ocean island basalts (OIB) and fate of subducted ocean crust (SOC) and mantle lithosphere (SML). *Episodes* **35**, 310-327.
- Ohtani, E., Kawabe, I., Moriyama, J., Nagata, Y. 1989.** Partitioning of elements between majorite garnet and melt and implications for petrogenesis of komatiite. *Contributions to Mineralogy and Petrology* **103**, 263-269.
- Pearce, J. A. 1982.** Trace element characteristics of lavas from destructive plate boundaries. *Andesites* **8**, 525-548.
- Pearce, J.A. Norry, M.J., 1979.** Petrogenetic implications of Ti, Zr, Y and Nb variations in volcanic rocks. *Contributions to Mineralogy and Petrology* **69**, 33-47.
- Pearce, J.A., 2008.** Geochemical fingerprinting of oceanic basalts with applications to ophiolite classification and the search for Archean oceanic crust. *Lithos* **100**, 14-48.
- Peate, D.W., Hawkesworth, C.J., Marta, M.S.M., Nick, W.R., Turner, S.P. 1999.** Petrogenesis and stratigraphy of the high-Ti/Y Urubici magma type in the Parana Flood Basalt Province and implications for the nature of Dupal-type mantle in the South Atlantic region. *Journal of Petrology* **40**, 451-473.
- Plume or subduction related? *Russian Journal of Earth Sciences* **5**, 93-100.
- Polat, A. 2012.** Growth of Archean continental crust in oceanic island arcs. *Geology* **40**, 383-384.
- Polat, A., Hofmann, A. W., Rosing, M. T. 2002.** Boninite-like volcanic rocks in the 3.7–3.8 Ga Isua greenstone belt, West Greenland: geochemical evidence for intra-oceanic subduction zone processes in the early Earth. *Chemical Geology* **184**, 231-254.
- Polat, A., Kerrich, R. 2006.** Reading the geochemical fingerprints of Archean hot subduction volcanic rocks: evidence for accretion and crustal recycling in a mobile tectonic regime. *American Geophysical Monograph* **164**, 189-213.

- Polat, A., Kerrich, R., Wyman, D. A. 1999.** Geochemical diversity in oceanic komatiites and basalts from the late Archean Wawa greenstone belts, Superior Province, Canada: trace element and Nd isotope evidence for a heterogeneous mantle. *Precambrian Research* **94**, 139-173.
- Puchtel, I. S., Haase, K. M., Hofmann, A. W., Chauvel, C., Kulikov, V. S., Garbe-Schönberg, C. D., Nemchin, A. A. 1997.** Petrology and geochemistry of crustally contaminated komatiitic basalts from the Vetreny Belt, southeastern Baltic Shield: evidence for an early Proterozoic mantle plume beneath rifted Archean continental lithosphere. *Geochimica et Cosmochimica Acta* **61**, 1205-1222.
- Puchtel, I. S., Humayun, M., Walker, R. J. 2007.** Os–Pb–Nd isotope and highly siderophile and lithophile trace element systematics of komatiitic rocks from the Volotsk suite, SE Baltic Shield. *Precambrian Research* **158**, 119-137.
- Ray, J., Saha, A., Koeberl, C., Thoni, M., Ganguly, S., Hazra, S. 2013.** Geochemistry and petrogenesis of Proterozoic mafic rocks from east Khasi Hills, Shillong Plateau, northeastern India. *Precambrian Research* **230**, 119-137.
- Reagan, M.K., Turner, S., Legg, M., Sims, K.W.W., Hards, V.L. 2008.** <sup>238</sup>U- and <sup>232</sup>Th-decay series constraints on the timescales of crystal fractionation to produce the phonolite erupted in 2004 near Tristan da Cunha, South Atlantic Ocean. *Geochimica et Cosmochimica Acta* **72**, 4367-4378.
- Reichow, M. K., Saunders, A. D., White, R. V., Al'Mukhamedov, A. I., Medvedev, A. Y. 2005.** Geochemistry and petrogenesis of basalts from the West Siberian Basin: an extension of the Permo–Triassic Siberian Traps, Russia. *Lithos* **79**, 425-452.
- Rollinson, H. 2007.** Recognizing early Archean mantle: a reappraisal. *Contrib. Mineral. Petrol.* **154**, 241–252.
- Rollinson, H. 2008.** Secular evolution of the continental crust: Implications for crust evolution models. *Geochemistry Geophysics Geosystems* **9**, Q12010. doi:10.1029/2008GC002262.
- Roy, A. B., Bhattacharya, H. N. 2012.** Tectonostratigraphic and geochronologic reappraisal constraining the growth and evolution of Singhbhum Archaean Craton, eastern India. *Journal of the Geological Society of India* **80**, 455-469.
- Rudnick, R.L., Gao, S. 2003.** Composition of the continental crust. *Treatise on geochemistry* **3**, 1-64.
- Safonova, I.Yu. 2009.** Intraplate magmatism and oceanic plate stratigraphy of the Paleo-Asian and Paleo-Pacific Oceans from 600 to 140 Ma, *Ore Geology Reviews* **35**, 137-154.
- Safonova, I.Yu., Simonov, V.A., Buslov, M.M., Ota, T., Maruyama, Sh. 2008.** Neoproterozoic basalts of the Paleo-Asian Ocean (Kurai accretion zone, Gorny Altai, Russia): geochemistry, petrogenesis, geodynamics. *Russian Geology and Geophysics* **49**, 254-271.
- Saha, A.K. 1994.** Crustal Evolution of Singhbhum-North Orissa, Eastern India, Memoir 27. *Geological Society of India*. 1-341.
- Saha, A.K., Ray, S.L., Sarkar, S.N. 1988.** Early history of the Earth: evidence from the eastern Indian shield. In: Mukhopadhyay, D. (Ed.), Precambrian of the Eastern Indian Shield. *Memoir Geological Society of India* **8**, pp. 13–37.

- Saha, A., Ganguly, S., Ray, J., Koeberl, C., Thöni, M., Sarbajna, C., Sawant, S. S. 2017.** Petrogenetic evolution of Cretaceous Samchampi-Samteran Alkaline Complex, Mikir Hills, Northeastern India: Implications on multiple melting events of heterogeneous plume and metasomatized sub-continental lithospheric mantle. *Gondwana Research*, **48**, 237-256.
- Saha, A., Manikyamba, C., Santosh, M., Ganguly, S., Khelen, A.C., Subramanyam, K.S.V. 2015.** Platinum Group Elements (PGE) geochemistry of komatiites and boninites from Dharwar Craton, India: Implications for mantle melting processes. *Journal of Asian Earth Sciences* **105**, 300-319.
- Saha, A., Santosh, M., Ganguly, S., Manikyamba, C., Ray, J., Datta, J. 2018.** Geochemical cycling during subduction initiation: Evidence from serpentinized mantle wedge peridotite in the south Andaman ophiolite suite, *Geoscience Frontiers*, <https://doi.org/10.1016/j.gsf.2017.12.01>.
- Said, N., Kerrich R., Groves, D. 2010.** Geochemical systematics of basalts of the Lower Basalt Unit, 2.7 Ga Kambalda sequence, Yilgran Craton, Australia: plume impingement at a rifted Craton margin. *Lithos* **115**, 82-100.
- Said, N., Kerrich, R. 2010.** Elemental and Nd-isotope systematics of the Upper Basalt Unit, 2.7 Ga Kambalda Sequence: Quantitative modeling of progressive crustal contamination of plume asthenosphere. *Chemical Geology* **273**, 193-211.
- Santosh, M. 2013.** Evolution of continents, cratons and supercontinents: building the habitable Earth. *Current Science* **104**, 871-879.
- Sarkar, S.N., Saha, A.K. 1962.** A revision of the Precambrian stratigraphy and tectonics of Singhbhum and adjacent regions. *Quart. J. Geol. Min. Met. SOC. India* **34**, 97-136
- Saunders, A.D., Norry, M.J., Tarney, J. 1988.** Origin of MORB and chemically-depleted mantle reservoirs: Trace element constrains. *Journal of Petrology (Special Lithosphere Issue)*, 415-445.
- Sengupta, S., Paul, D.K., DE Laeter, J.R., McNaughton, N.J., Bandyopadhyay, P.K. DE Smeth, J.B. 1991.** Mid-Archaean evolution of the eastern Indian craton: geochemical and isotopic evidence from the eastern Indian craton. *Contributions to Mineralogy and petrology* **117**, 45-55.
- Sharan, A.K. 1983,** Geochemical study of Precambrian granitic rocks around Chakradharpur, District Singhbhum, Bihar. Unpublished Ph.D. thesis, Patna University, Patna
- Sharma, M., Basu, A.R., Ray, S.L. 1994.** Sm-Nd isotopic and geochemical study of the Archean Tonalite-Amphibolite association from the eastern Indian Craton. *Contributions to Mineralogy and Petrology* **117**, 45-55.
- Sharma, R.S. 2009.** Cratons and Fold Belts of India. Springer Verlag, Heidelberg, 324pp.
- Shellnutt, J.G., Bhat, G.M., Wang, K., Brookfield, M.E., Jahn, B., Dostal, J. 2014.** Petrogenesis of the flood basalts from the Early Permian Panjal Traps, Kashmir, India: Geochemical evidence for shallow melting of the mantle. *Lithos* **204**, 159-171.
- Simonov V.A., Mikolaichuk A.V., Safonova I.Yu., Kotlyarov A.V., Kovyazin S.V. 2014.** Late Paleozoic-Cenozoic intra-plate continental basaltic magmatism of the Tianshan-Junggar region in the SW Central Asian Orogenic Belt. *Gondwana Research*, <http://dx.doi.org/10.1016/j.gr.2014.03.001>

- Singh, M. R., Manikyamba, C., Ganguly, S., Ray, J., Santosh, M., Singh, T.D., Chandan Kumar, B. 2017.** Paleoproterozoic arc basalt-boninite-high magnesian andesite-Nb enriched basalt association from the Malangtoli volcanic suite, Singhbhum Craton, eastern India: Geochemical record for subduction initiation to arc maturation continuum. *Journal of Asian Earth Sciences* **134**,191-206.
- Singh, M. R., Manikyamba, C., Ray, J., Ganguly, S., Santosh, M., Saha, A., Rambabu, S., Sawant, S. S., 2016.** Major, trace and platinum group element (PGE) geochemistry of Archean Iron Ore Group and Proterozoic Malangtoli metavolcanic rocks of Singhbhum Craton, Eastern India: Inferences on mantle melting and sulphur saturation history. *Ore Geology Reviews***72**, 1263-1289.
- Sleep, N. H. 2006.** Mantle plumes from top to bottom. *Earth-Science Reviews* **77**, 231-271
- Sleep, N. H., Ebinger, C. J., Kendall, J. M. 2002.** Deflection of mantle plume material by cratonic keels. *Geological Society, London, Special Publications* **199**, 135-150.
- Smithies, R.H., Champion, D.C., Cassidy, K.F. 2003.** Formation of Earth's early Archaean continental crust. *Precambrian Research***127**, 89-101.
- Smithies, R.H., Champion, D.C., Van Kranendonk, M. J. 2009.** Formation of Paleoproterozoic continental crust through infracrustal melting of enriched basalt. *Earth and Planetary Science Letters* **281**, 298-306.
- Smithies, R.H., Champion, D.C., van Kranendonk, M.K., Howard, H.M., Hickman, A.H. 2005.** Modern-style subduction processes in the Mesoarchean: geochemical evidence from the 3.12 Ga Whundo intra-oceanic arc. *Earth and Planetary Science Letters***231**, 221–237. doi:10.1016/j.epsl.2004.12.026.
- Song, X-Y., Qi, H-W., Robinson, P.T., Zhou, M-F., Cao, Z-M., Chen L-M. 2008.** Melting of the subcontinental lithospheric mantle by the Emeishan mantle plume; evidence from the basal alkaline basalts in Dongchuan, Yunnan, Southwestern China. *Lithos* **100**, 93-111.
- Song, X-Y., Zhou, M-F., Hou, Z-Q., Cao, Z-M., Wang, Y-L., Li, Y. 2001.** Geochemical Constraints on the Mantle Source of the Upper Permian Emeishan Continental Flood Basalts, Southwestern China. *International Geology Review* **43**, 213-225.
- Sproule, R.A., Leshner, C.M., Ayer, J.A., Thurston, P.C., Herzberg, C.T. 2002.** Spatial and temporal variations in the geochemistry of komatiites and komatiitic basalts in the Abitibi Greenstone Belt. *Precambrian Research* **115**, 153–186.
- Stern, R. A., Syme, E. C., Bailes, A. H., Lucas, S. B. 1995.** Paleoproterozoic (1.90–1.86 Ga) arc volcanism in the Flin Flon Belt, Trans-Hudson Orogen, Canada. *Contributions to Mineralogy and Petrology* **119**, 117-141.
- Sun, S.S., McDonough, W.F. 1989.** Chemical and isotopic systematics of oceanic basalts: implications for mantle composition and processes. In: Saunders, A.D., Norry, M.J. (Eds.), 1989. Magmatism in the Ocean Basins 42. *Geological Society of London Special Publication*, pp. 313-345.
- Taylor, S.R., McLennan, S.M. 1995.** The geochemical evolution of the continental crust. *Rev. Geophys.***33**, 241–265.

- Touret, J. L. R., Santosh, M., Huizenga, J. M. 2016.** High-temperature granulites and supercontinents. *Geoscience Frontiers* **7**, 101-113.
- Turkina, O.M., Nozhkin, A.D. 2003.** Genesis of Archean tonalite–trondhjemite suites: Plume or subduction related? *Russian Journal of Earth Sciences* **5**, 93-100
- Viljoen, M.J., Viljoen, R.P. 1969** The geology and geochemistry of the lower ultramafic unit of the Onvarwacht Group and a proposed new class of igneous rocks. *Geol. Soc. South Africa Spec. Pub.* **2**, 221-244.
- Walter, M.J. 1998.** Melting of garnet peridotite and the origin of komatiite and depleted lithosphere. *Journal of Petrology* **39**, 29-60.
- Weaver, B.L. 1990.** Geochemistry of highly-undersaturated ocean island basalt suites from the South Atlantic Ocean: Fernando de Noronha and Trindade Islands. *Contributions to Mineralogy and Petrology* **105**, 502-515.
- Wyman, D. 2018.** Do cratons preserve evidence of stagnant lid tectonics? *Geoscience Frontiers* **9**, 3-17.
- Wyman, D.A. 2013.** A critical assessment of Neoproterozoic "plume only" geodynamics: Evidence from the Superior Province. *Precambrian Research* **229**, 3-19.
- Wyman, D.A., Kerrich, R. 2009.** Plume and arc magmatism in the Abitibi subprovince: Implications for the origin of Archean continental lithospheric mantle. *Precambrian Research* **168**, 4-22.
- Xu, Y-G., Ma, J-L., Frey, F.A., Feigenson, M.D., Liu, J-F. 2005.** Role of lithosphere–asthenosphere interaction in the genesis of Quaternary alkali and tholeiitic basalts from Datong, western North China Craton. *Chemical Geology* **224**, 247-271.
- Yang, Q.Y., Santosh, M., Shen, J.F., Li, S.R. 2014.** Juvenile vs. recycled crust in NE China: Zircon U–Pb geochronology, Hf isotope and an integrated model for Mesozoic gold mineralization in the Jiadong Peninsula. *Gondwana Research* **25**, 1445-1468.
- Yaxley, G. 2000.** Experimental study of the phase and melting relations of homogeneous basalt + peridotite mixtures and implications for the petrogenesis of flood basalts. *Contributions to Mineralogy and Petrology* **139**, 326-338.
- Zhai, M.G., Santosh, M. 2011.** The early Precambrian odyssey of the North China Craton: a synoptic overview. *Gondwana Research* **20**, 6–25.
- Zhai, M.G., Santosh, M. 2013.** Metallogeny of the North China Craton: link with secular changes in the evolving Earth. *Gondwana Research* **24**, 275-297.
- Zhao, J.J., Zhou, M.F. 2007.** Geochemistry of Neoproterozoic mafic intrusions in the Panzhihua district (Sichuan Province, SW China): implications for subduction related metasomatism in the upper mantle. *Precambrian Research* **152**, 27-47.

## Figure Captions

**Fig. 1** Simplified geological map of Singhbhum Craton (modified after Saha, 1994; Manikyamba et al., 2015)

### **Fig.2**

Geological map of the study area showing the occurrence of ultramafic enclaves within Chakradharpur granite gneiss.

### **Fig.3**

- A.** Photomicrograph showing randomly oriented short prismatic crystals and fibers of actinolite (Act) (low birefringent) cross-cut by a few needles of strongly birefringent tremolite (Tr) showing relict igneous texture - an altered ultramafic rock (meta-komatiite). The rock contains minor amount of titanite. Locality: Asantalia, northwest of Chakradharpur; between crossed polars
- B.** BSE image of meta-komatiite, containing a large oval-shaped porphyroblast of phlogopite (Phl) rimmed with titanite (Ttn) in tremolite-actinolite schist.
- C.** BSE image showing random orientation of tremolite (Tr) and actinolite (Act) in meta-komatiite indicating derivation from igneous protolith
- D.** Photomicrograph showing magnified view of transformation of clinopyroxene (Cpx) to amphibole with deformation of cleavages in ultramafic enclaves. White coloured talc (Tlc) is derived from alteration of magnesium-rich parent mineral
- E.** Photomicrograph showing magnified view of long and curved prisms of cummingtonite (Cum) occurring in talc (Tlc) in ultramafic rock under crossed polars flanked on either side by amphiboles
- F.** Photomicrograph showing micro-folding in amphiboles (Amp) in ultramafic rocks associated with talc (Tlc) under crossed polars
- G.** Photomicrograph showing dendritic-spinifex texture and pressure solution fractures in komatiitic enclave
- H.** Photomicrograph showing crenulation cleavage in komatiitic enclave
- I.** Photomicrograph showing sub-ophitic texture in meta-gabbro enclave
- J.** Photomicrograph showing occurrence of strained quartz in metasedimentary enclave
- K.** Photomicrograph showing occurrence of quartz (Qz), sericite (Ser), titanite (Ttn) and zircon (Zrn) in metasedimentary enclave
- L.** Photomicrograph showing occurrence of broken zircon grain in metasedimentary enclave

### **Fig.4**

Total alkali vs. silica diagram for the studied rocks (after Le Bas et al., 2000) occurring as xenoliths in the Proterozoic Chakradharpur granites, Singhbhum craton

### **Fig.5**

Chondrite normalized REE patterns and primitive mantle-normalized multi-element plots for the studied rocks. Normalizing factors are from Sun and McDonough (1989)

### **Fig.6**

- A.** Th/Yb vs. Nb/Yb plots (after Pearce, 2008) for the studied xenoliths showing tholeiitic lineage



- B.  $(\text{Gd}/\text{Yb})_n$  vs.  $\text{Al}_2\text{O}_3/\text{TiO}_2$  diagram showing fields for Archean Barberton and Munro type komatiites, Phanerozoic Gorgona komatiites, Phanerozoic boninites and plots for xenoliths from present study
- C. Zr/Nb vs. Nb/Th plot reflecting role of hydrated mantle for the generation of the studied rock (after Condie, 2015)

**Fig.7**

- A. Dy/Yb vs. La/Yb plot for the studied ultramafic xenoliths indicating their generation at shallower depth in the spinel-peridotite stability field
- B. Sm/Yb vs. Sm plot (after Zhao and Zhou, 2007) corresponding to 10–20% melting of spinel lherzolite mantle. Melting curves are after Aldanmaz *et al.* (2000). DM and PM represents depleted and primitive mantle respectively. A pair of mode and melt mode curves are drawn for spinel (Kinzler, 1997) and garnet (Walter, 1998) lherzolite

**Fig.8**

Cartoon showing schematic model for the generation of studied xenoliths at rifted cratonic margin. See text for discussion.

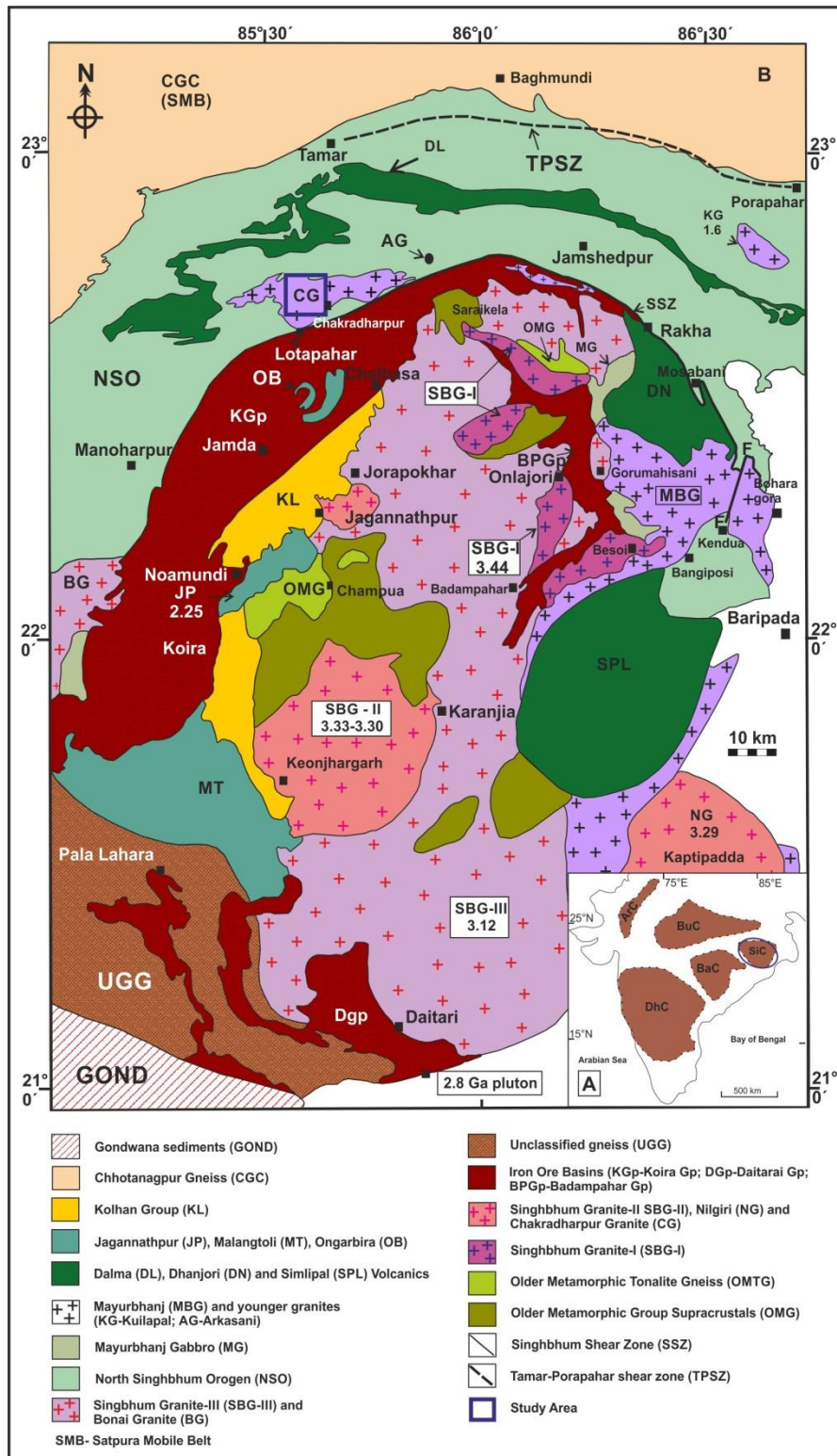


Figure 1

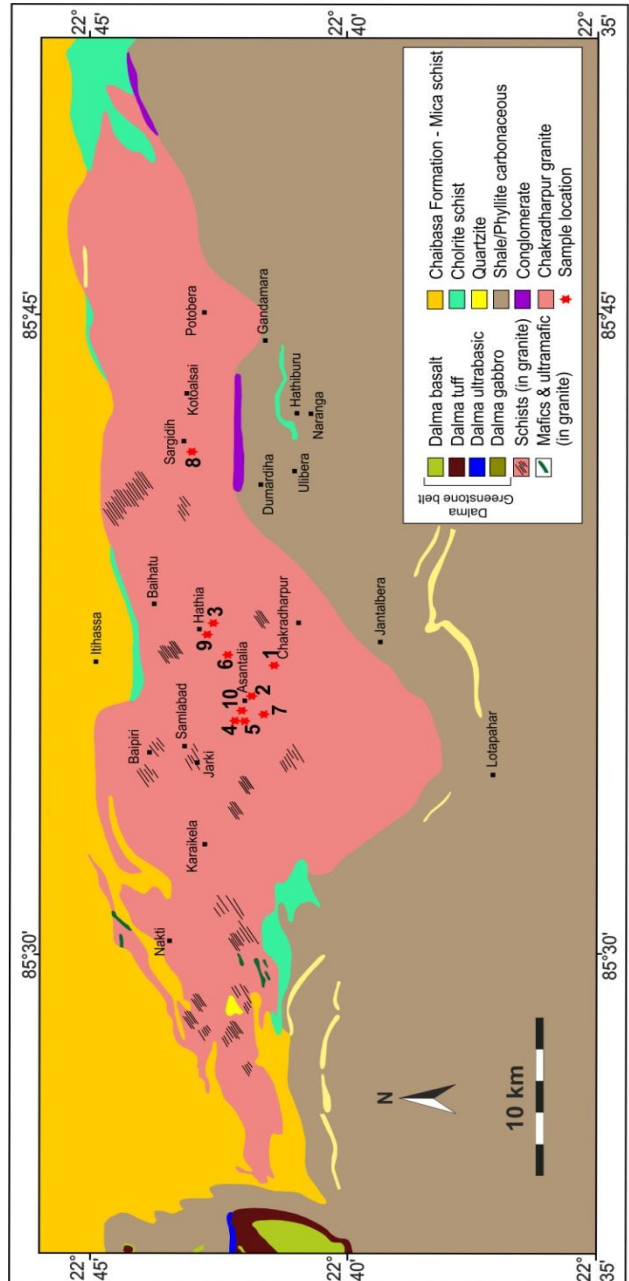


Figure 2

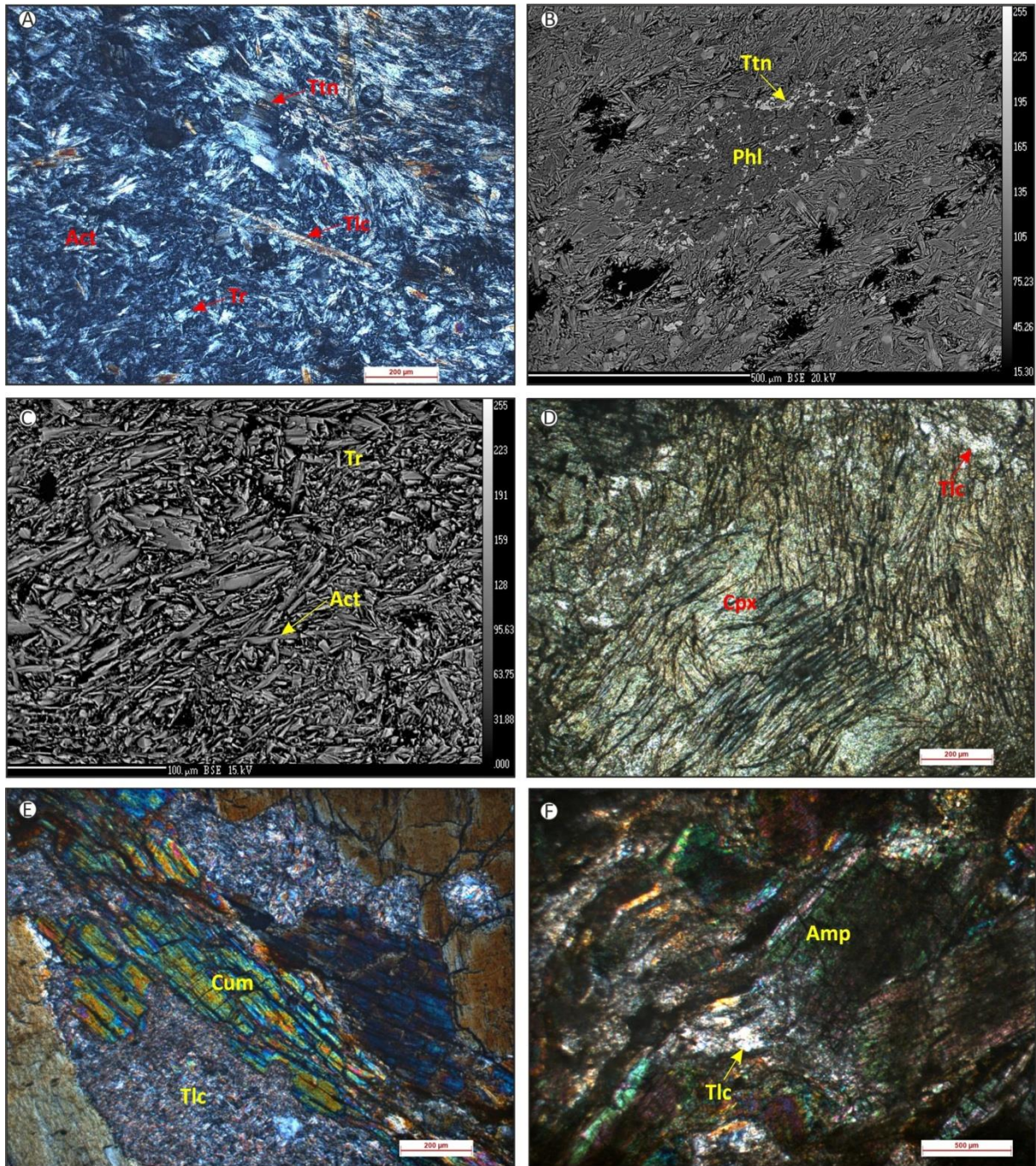


Figure 3

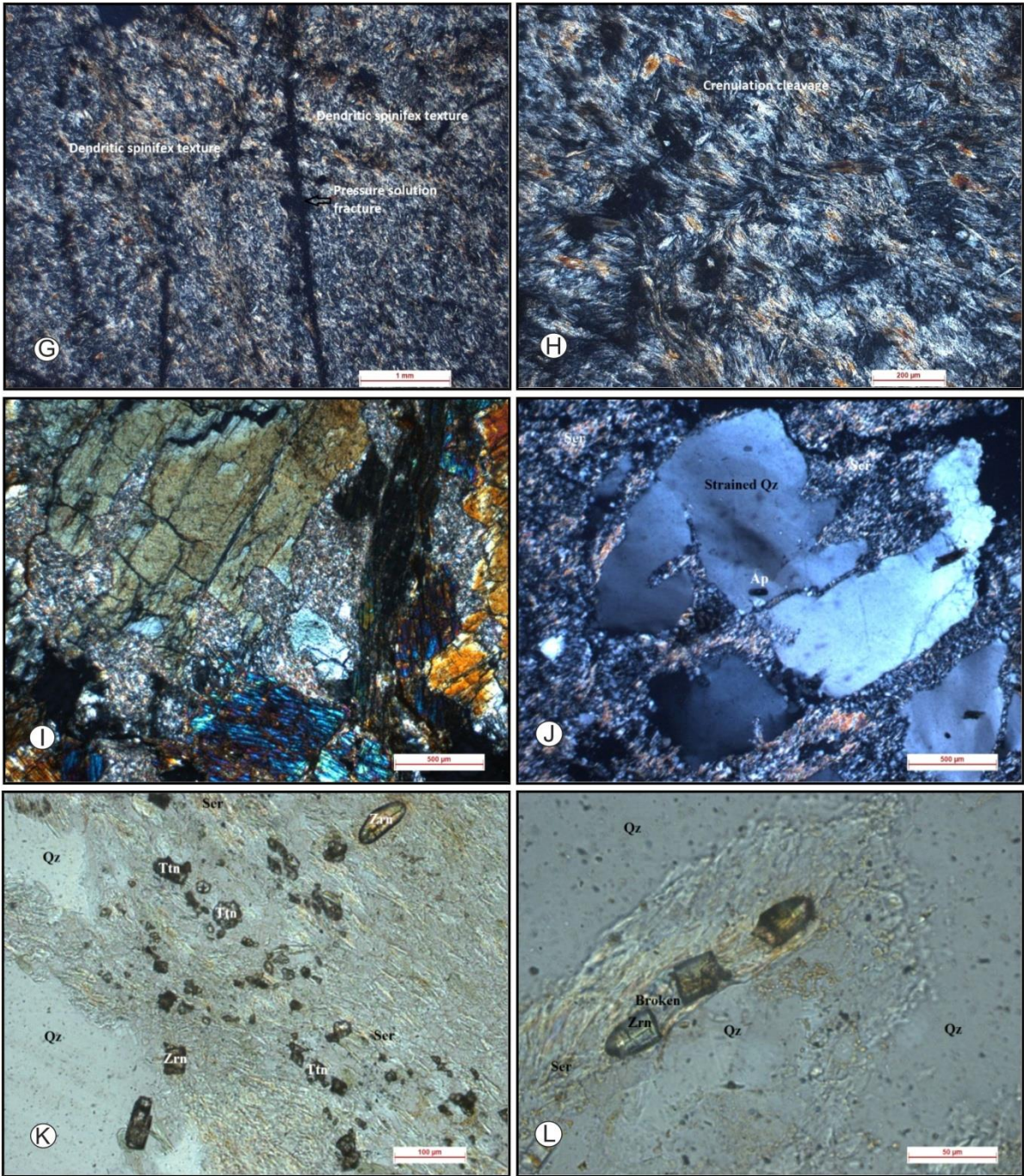


Figure 3 Contd...

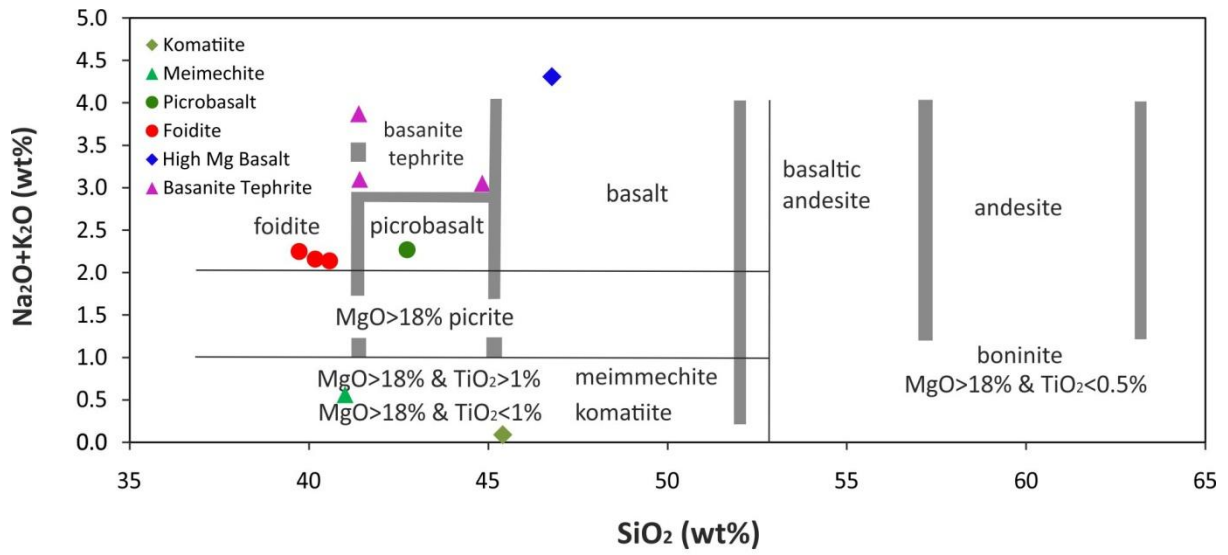


Figure 4

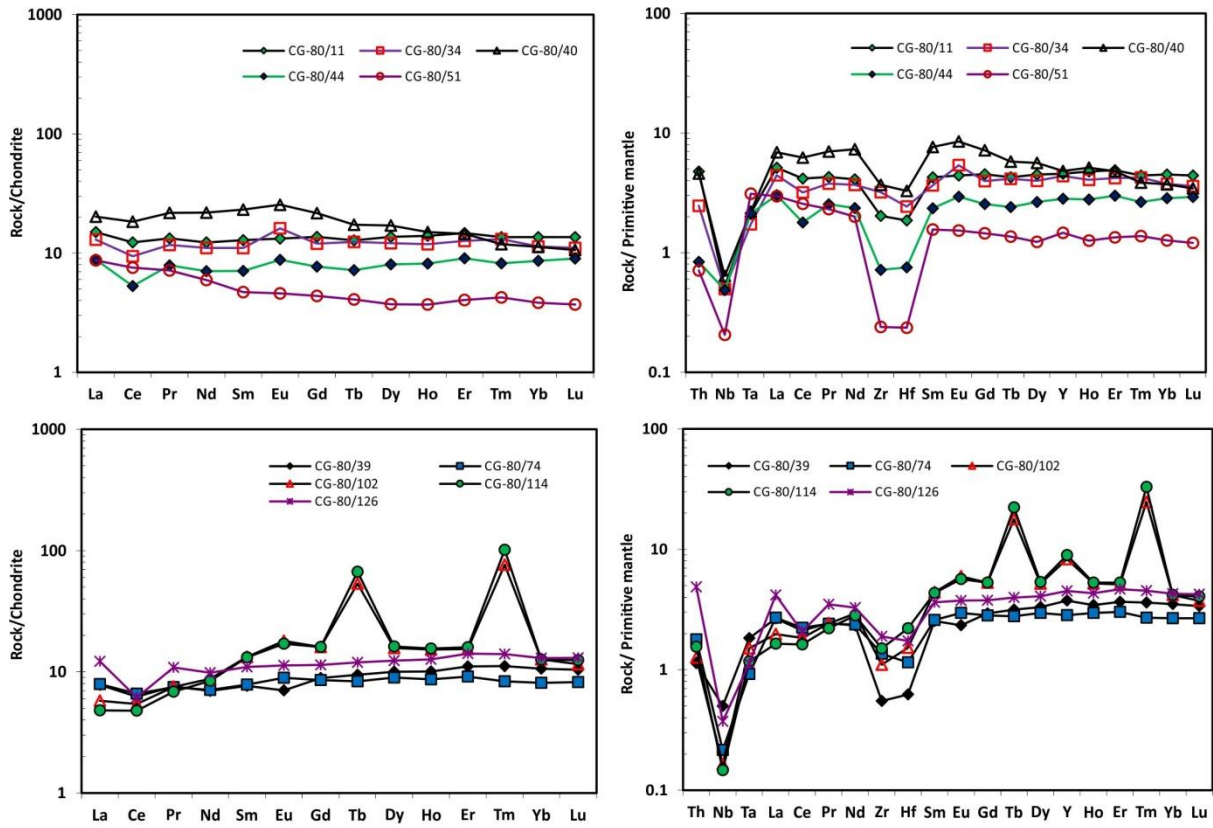


Figure 5

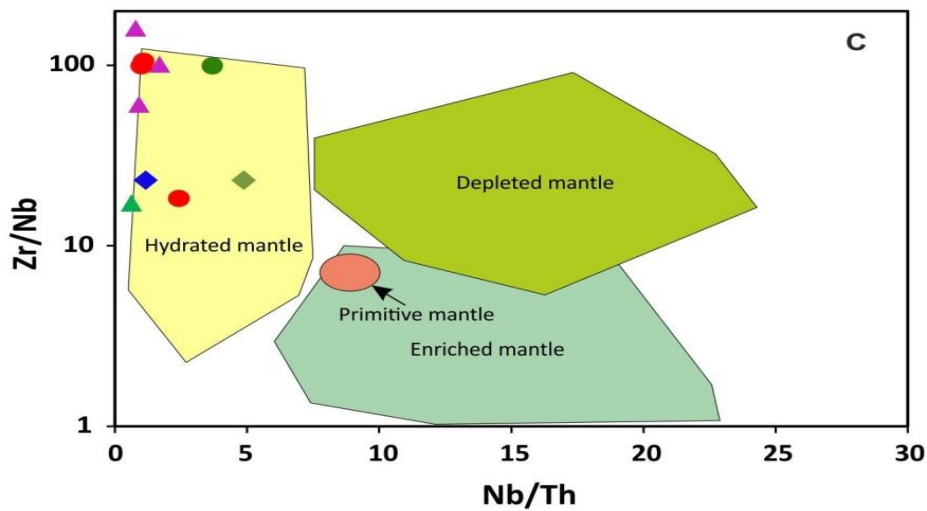
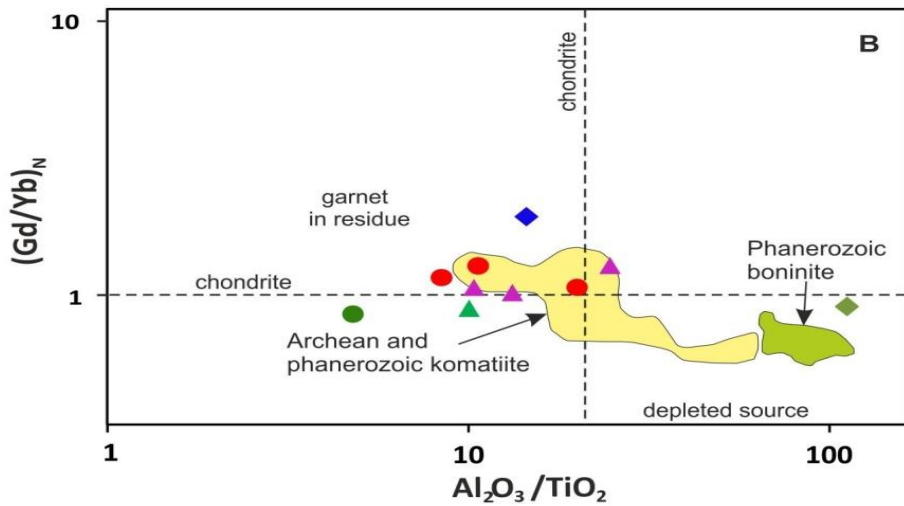
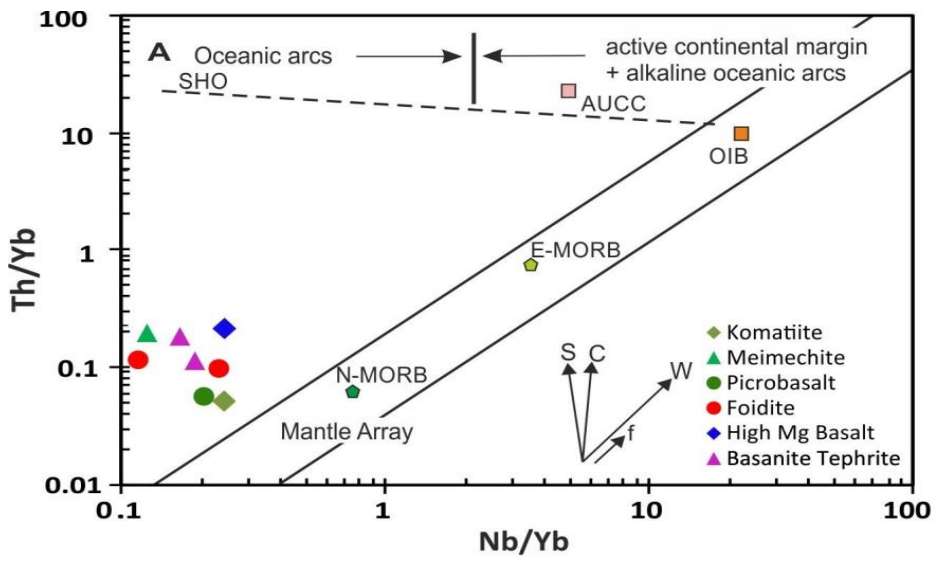


Figure 6



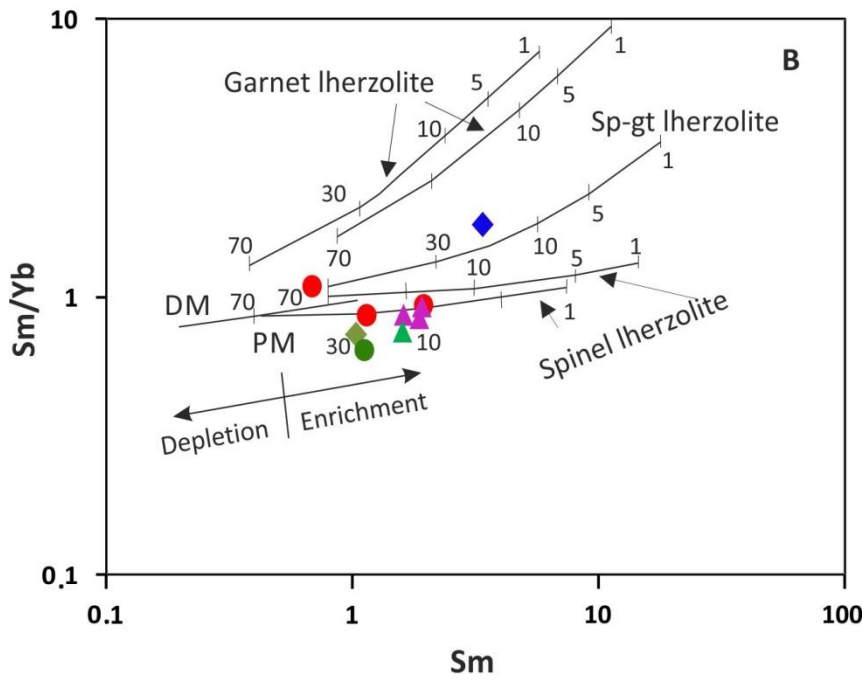
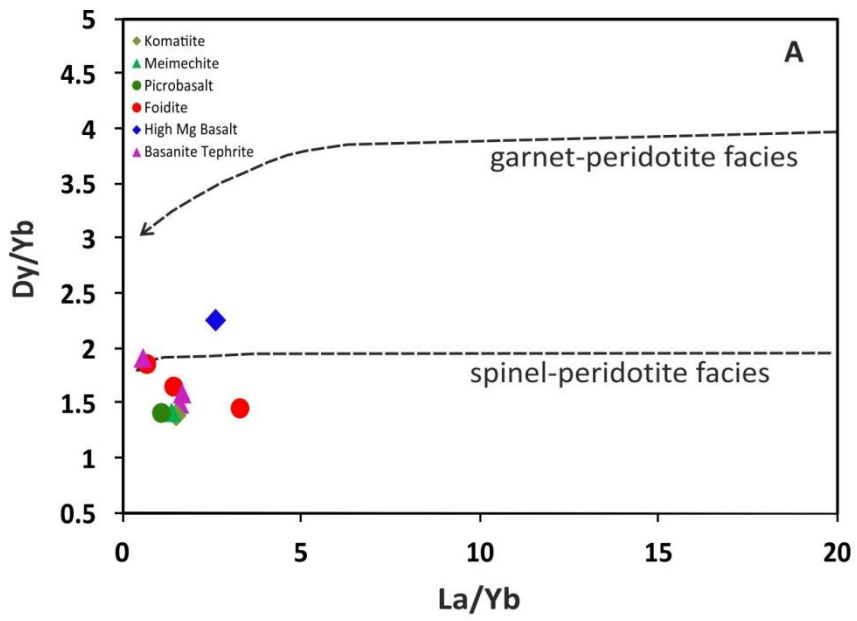


Figure 7

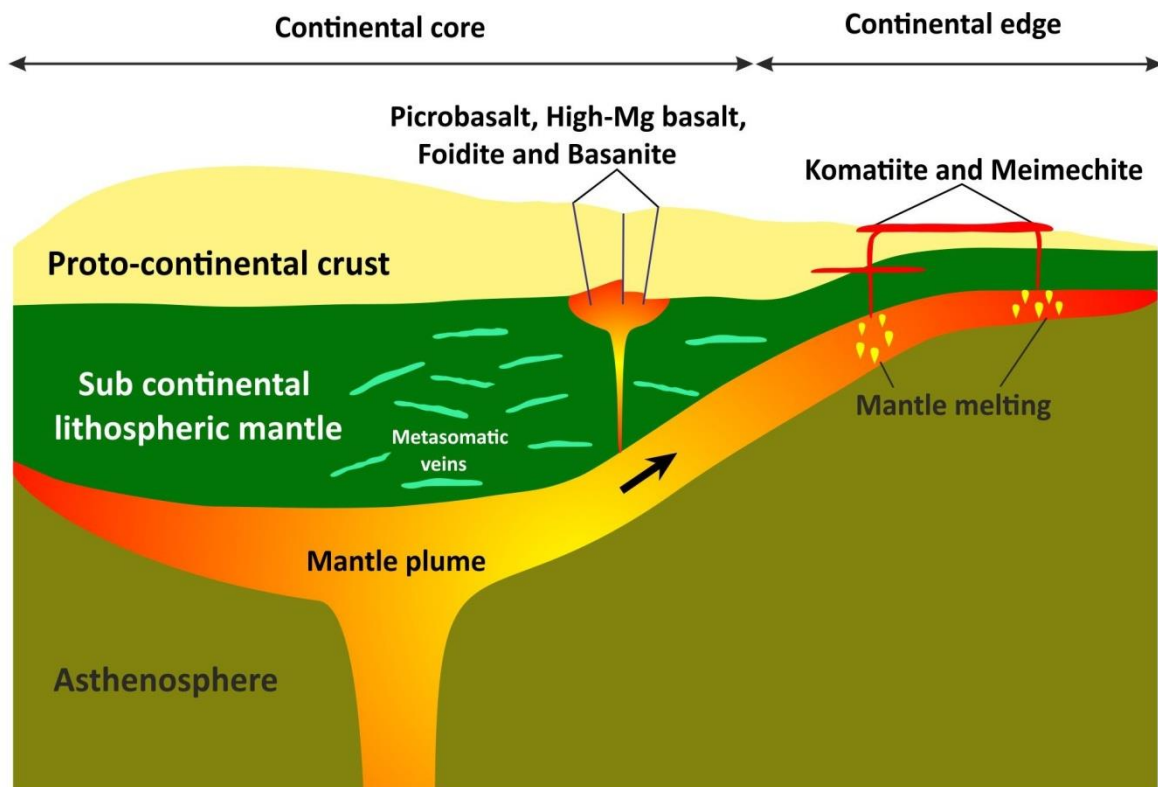


Figure 8

**Table 1.** Stratigraphy of the Singbhum craton, Eastern India (after Saha et al., 1988; Mishra, 2006; Manikymba et al., 2015).

Stratigraphic unit	Geological events	Major lithologies	Age (Ga)
Newer Dolerite dykes and sills- phase I, II and III	Intrusion of dykes and sills	quartz dolerite,	~2.0–1.0
Kolhan Group	Deposition of sediments	Phyllite, limestone, sandstone-conglomerate	~2.25
Jagannathpur and Malangtoli lavas	Volcanic eruption	Basalt, basaltic andesite	~2.25
Dhanjori and Dalma volcanics, Tamperkola granite	Mafic volcanism and felsic plutonism	Ultramafic- mafic tuffs, basalts, quartzite-conglomerate High Mg- lavas, pyroclastic rocks, granite	~2.80
	<i>Thermal metamorphism of OMG, OMTG, SBG-II and SBG-III</i>		~3.07-3.05
Mayurbhanj Granite and Gabbro (MBG)	Coeval emplacement of MBG	Granite, gabbro, pierite, anorthosite	~3.09
Simlipal lavas and metasediments	Formation of volcano-sedimentary basin	Spillites, tuffs, quartzites	> 3.09
Singbhum Group	Formation and deformation of supracrustals sedimentation and magmatism	Pelites, felsic volcanic, mafic sills	~3.12-3.09
	----- <i>Unconformity</i> -----		
	<i>Thermal metamorphism of OMG due to SBG-III and Bonai granite emplacement</i>		~3.16-3.10
SBG- III (~Chakradharpur Granite)	Emplacement of SBG- III and Chakradharpur Granite	Granodiorite, granite	~3.12
Bonai Granite	Plutonic emplacement	Granite, granodiorite	~3.16
	<i>Metamorphism of OMG, OMTG and IOG rocks</i>		~3.24-3.20
Iron Ore Group (IOG)	Formation, structural deformation (folding) and metamorphism of IOG rocks	Mafic and felsic lavas, tuffs, shales, BHJ, BHQ, quartzite, dolomite, conglomerate	~3.30-3.16
	----- <i>Unconformity</i> -----		
	<i>Thermal metamorphism of OMG and OMTG due to SBG-II and Nilgiri granite emplacement</i>		~3.30
Nilgiri Granite	Emplacement of Nilgiri Granite	Tonalite, Granite	~3.29
SBG-II	Emplacement of SBG-II	Granodiorite	~3.33- 3.30
Singbhum Granite (SBGI)	Emplacement of granitoid plutons	Tonalite, Granodiorite	~3.44- ~3.38
Older Metamorphic Tonalite Gneiss (OMTG)	Folding of OMG supracrustals and synkinematic intrusion of tonalite	Tonalite gneiss, granodiorite	~3.44- 3.42
Older Metamorphic Group (OMG)	Deposition of sediments with mafic volcanism and plutonism	Pelitic schists, banded calc-gneiss, amphibolites	~3.55-3.44
Unstable sialic crust		Sialic sediments	3.6 - 3.55

**Table 2** Major and trace element compositions of studied rocks occurring as enclaves in the Chakradharpur granites, Singhbhum Craton, India

	CG-80/11	CG-80/34	CG-80/114	CG-80/40	CG-80/44	CG-80/126
	BasaniteTephrite			High Mg Basalt	Komatiite	Meimechite
<i>wt%</i>						
SiO <sub>2</sub>	41.41	41.39	44.83	46.77	45.40	41.00
TiO <sub>2</sub>	0.80	1.29	0.34	1.09	0.09	1.15
Al <sub>2</sub> O <sub>3</sub>	10.69	13.43	8.53	15.93	10.46	11.62
Fe <sub>2</sub> O <sub>3</sub> <sup>(T)</sup>	9.51	7.73	7.40	8.99	8.67	10.21
MnO	0.14	0.10	0.12	0.06	0.09	0.08
MgO	24.68	23.00	24.46	20.74	28.14	24.77
CaO	8.17	4.84	9.82	0.14	6.07	1.99
Na <sub>2</sub> O	1.97	0.92	0.90	0.03	0.05	0.31
K <sub>2</sub> O	1.13	2.95	2.15	4.28	0.04	0.25
P <sub>2</sub> O <sub>5</sub>	0.12	0.28	0.10	0.08	0.03	0.08
LOI	1.63	4.05	1.77	2.06	1.09	7.69
Total	100.25	99.98	100.42	100.17	100.13	99.15
Na <sub>2</sub> O+K <sub>2</sub> O	3.10	3.87	3.05	4.31	0.09	0.56
<i>ppm</i>						
Cr	351	416	340	661	1122	171
Co	59	49	80	58	50	51
Ni	199	236	261	423	258	143
Rb	35.8	61.4	6.2	26.1	39.6	8.5
Sr	55.5	24.8	64.8	110.2	30.5	9.1
Cs	0.9	0.9	3.6	1.5	0.5	1.0
Ba	72	202	28	40	144	20
Sc	42.26	37.00	53.06	30.19	35.45	45.30
V	363	252	610	474	278	361
Nb	0.37	0.35	0.10	0.45	0.35	0.27
Ta	0.09	0.07	0.05	0.09	0.09	0.05
Zr	22.66	35.91	16.83	41.25	8.02	21.18
Hf	0.57	0.75	0.68	1.01	0.23	0.54
Th	0.41	0.21	0.13	0.39	0.07	0.41
U	0.15	0.06	0.10	0.19	0.05	0.21
Y	20.82	19.87	40.74	21.90	12.86	20.48

**Table 2**Contd...

	CG-80/11	CG-80/34	CG-80/114	CG-80/40	CG-80/44	CG-80/126
	BasaniteTephrite			High Mg Basalt	Komatiite	Meimechite
La	3.52	3.05	1.13	4.75	2.08	2.86
Ce	7.40	5.67	2.88	11.08	3.19	3.70
Pr	1.18	1.04	0.61	1.94	0.70	0.97
Nd	5.55	4.98	3.81	9.86	3.18	4.43
Sm	1.89	1.62	1.93	3.40	1.04	1.61
Eu	0.74	0.90	0.95	1.43	0.49	0.63
Gd	2.69	2.36	3.15	4.27	1.52	2.25
Tb	0.46	0.45	2.41	0.62	0.26	0.43
Dy	3.32	2.94	3.93	4.14	1.95	3.00
Ho	0.78	0.67	0.87	0.84	0.46	0.71
Er	2.35	2.02	2.54	2.30	1.44	2.24
Tm	0.33	0.31	2.43	0.28	0.20	0.34
Yb	2.22	1.85	2.06	1.84	1.41	2.11
Lu	0.33	0.27	0.30	0.25	0.22	0.31
Cu	41.92	58.80	107.29	64.11	23.68	49.30
Zn	90.36	99.10	147.27	69.13	87.52	76.63
Ga	22.27	20.01	25.65	29.16	16.94	22.18
Pb	11.67	9.08	13.52	10.59	8.83	15.59
Al <sub>2</sub> O <sub>3</sub> /TiO <sub>2</sub>	13.36	10.41	25.09	14.61	116.22	10.10
CaO/Al <sub>2</sub> O <sub>3</sub>	0.76	0.36	1.15	0.01	0.58	0.17
K <sub>2</sub> O/P <sub>2</sub> O <sub>5</sub>	9.42	10.54	21.50	53.50	1.33	3.13
TiO <sub>2</sub> /P <sub>2</sub> O <sub>5</sub>	6.67	4.61	3.40	13.63	3.00	14.38
Zr/Hf	39.54	47.78	24.66	40.68	34.49	39.43
Zr/Nb	60.89	101.49	160.81	90.79	23.11	79.75
Th/Ta	4.62	2.96	2.74	4.31	0.82	8.96
Th/Ce	0.05	0.04	0.05	0.04	0.02	0.11
Nb/Ta	4.23	4.99	2.18	5.03	4.00	5.73
Zr/Sm	11.99	22.11	8.72	12.14	7.69	13.15
Dy/Yb	1.50	1.59	1.91	2.25	1.39	1.42
Zr/Ba	0.32	0.18	0.61	1.03	0.06	1.08
Nb/Th	0.92	1.69	0.79	1.17	4.88	0.64
La/Nb	9.47	8.63	10.81	10.45	5.99	10.78
(La/Yb) <sub>n</sub>	1.10	1.14	0.38	1.79	1.03	0.94
(Gd/Yb) <sub>n</sub>	1.00	1.05	1.27	1.92	0.89	0.88
(La/Sm) <sub>n</sub>	1.17	1.18	0.37	0.87	1.25	1.11
(La/Nb) <sub>n</sub>	9.83	8.96	11.22	10.85	6.21	11.18
(Nb/La) <sub>pm</sub>	0.10	0.11	0.09	0.09	0.16	0.09
(Th/La) <sub>pm</sub>	0.93	0.56	0.94	0.66	0.28	1.17
(Nb/Th) <sub>pm</sub>	0.11	0.20	0.09	0.14	0.58	0.08
(Th/Nb) <sub>pm</sub>	9.16	4.97	10.55	7.20	1.72	13.11

Normalization after Sun and McDonough (1989)

**Table 2Contd...**

	CG-80/39	CG-80/74	CG-80/102	CG-80/51
	Picrobasalt	Foidite		
<i>wt%</i>				
SiO <sub>2</sub>	42.73	39.72	40.17	40.57
TiO <sub>2</sub>	1.89	0.49	0.99	1.10
Al <sub>2</sub> O <sub>3</sub>	9.01	9.94	10.60	9.30
Fe <sub>2</sub> O <sub>3</sub> <sup>(T)</sup>	9.51	8.55	9.34	9.54
MnO	0.12	0.11	0.13	0.13
MgO	23.84	24.88	24.70	24.60
CaO	8.69	7.64	10.06	9.57
Na <sub>2</sub> O	1.64	2.20	1.92	1.94
K <sub>2</sub> O	0.63	0.05	0.24	0.20
P <sub>2</sub> O <sub>5</sub>	0.19	0.06	0.09	0.10
LOI	0.99	4.62	1.61	3.45
Total	99.24	98.26	99.85	100.50
Na <sub>2</sub> O+K <sub>2</sub> O	2.27	2.25	2.16	2.14
<i>ppm</i>				
Cr	866	245	366	1770
Co	53	59	86	57
Ni	228	294	259	992
Rb	38.0	0.9	6.2	1.6
Sr	14.3	65.4	47.4	8.0
Cs	0.6	0.1	3.2	0.1
Ba	81	24	27	7
Sc	37.78	31.13	56.38	18.60
V	187	285	570	66
Nb	0.36	0.15	0.12	0.15
Ta	0.07	0.04	0.06	0.13
Zr	6.15	15.20	12.33	2.68
Hf	0.19	0.36	0.47	0.07
Th	0.10	0.15	0.11	0.06
U	0.09	0.06	0.07	0.04
Y	17.06	12.91	37.62	6.67

**Table 2***Contd...*

	CG-80/39	CG-80/74	CG-80/102	CG-80/51
	Picrobasalt	Foidite		
La	1.83	1.86	1.36	2.04
Ce	3.76	3.98	3.27	4.56
Pr	0.68	0.67	0.67	0.64
Nd	3.14	3.20	3.95	2.69
Sm	1.13	1.15	1.96	0.69
Eu	0.39	0.50	1.00	0.26
Gd	1.75	1.68	3.15	0.86
Tb	0.34	0.30	1.92	0.15
Dy	2.44	2.18	3.82	0.91
Ho	0.56	0.49	0.85	0.21
Er	1.76	1.45	2.45	0.64
Tm	0.27	0.20	1.83	0.10
Yb	1.73	1.32	2.06	0.62
Lu	0.25	0.20	0.28	0.09
Cu	44.09	42.43	104.83	35.61
Zn	84.79	41.81	118.37	61.61
Ga	15.90	19.90	25.97	7.60
Pb	9.00	10.43	13.94	8.63
Al <sub>2</sub> O <sub>3</sub> /TiO <sub>2</sub>	4.77	20.29	10.71	8.45
CaO/Al <sub>2</sub> O <sub>3</sub>	0.96	0.77	0.95	1.03
K <sub>2</sub> O/P <sub>2</sub> O <sub>5</sub>	3.32	0.83	2.67	2.00
TiO <sub>2</sub> /P <sub>2</sub> O <sub>5</sub>	9.95	8.17	11.00	11.00
Zr/Hf	31.89	42.64	26.25	36.74
Zr/Nb	17.27	98.98	105.16	18.26
Th/Ta	1.29	4.01	1.73	0.47
Th/Ce	0.03	0.04	0.03	0.01
Nb/Ta	4.75	4.06	1.89	1.15
Zr/Sm	5.46	13.21	6.30	3.87
Dy/Yb	1.41	1.65	1.85	1.45
Zr/Ba	0.08	0.62	0.46	0.39
Nb/Th	3.70	1.01	1.09	2.43
La/Nb	5.14	12.11	11.58	13.90
(La/Yb) <sub>n</sub>	0.74	0.98	0.46	2.27
(Gd/Yb) <sub>n</sub>	0.84	1.05	1.26	1.14
(La/Sm) <sub>n</sub>	1.02	1.01	0.43	1.84
(La/Nb) <sub>pm</sub>	5.33	12.57	12.01	14.42
(Nb/La) <sub>pm</sub>	0.19	0.08	0.08	0.07
(Th/La) <sub>pm</sub>	0.43	0.66	0.64	0.24
(Nb/Th) <sub>pm</sub>	0.44	0.12	0.13	0.29
(Th/Nb) <sub>pm</sub>	2.27	8.28	7.68	3.45

Normalization after Sun and McDonough (1989)